Geochemistry, Geophysics, Geosystems®

AGU ADVANCING EARTH AND SPACE SCIENCE

RESEARCH ARTICLE
10.1029/2021GC009999

Rapid Assembly and Eruption of a Shallow Silicic Magma Reservoir, Reyðarártindur Pluton, Southeast Iceland

E. L. Rhodes[1,2], A. K. Barker[1,2], S. Burchardt[1,2], C. F. Hieronymus[1], S. N. Rousku[1], D. W. McGarvie[3], T. Mattsson[4,5], T. Schmiedel[1], E. Ronchin[6], and T. Witcher[1]

[1]Department of Earth Sciences, Uppsala University, Uppsala, Sweden, [2]Center for Natural Hazards and Disaster Science, Uppsala University, Uppsala, Sweden, [3]Lancaster Environment Centre, Lancaster University, Lancaster, UK, [4]School of Earth and Environmental Sciences, University of St Andrews, St Andrews, UK, [5]Department of Geological Sciences, Stockholm University, Stockholm, Sweden, [6]Department of Earth Sciences, Sapienza University of Rome, Rome, Italy

Abstract Although it is widely accepted that shallow silicic magma reservoirs exist, and can feed eruptions, their dynamics and longevity are a topic of debate. Here, we use field mapping, geochemistry, 3D pluton reconstruction and a thermal model to investigate the assembly and eruptive history of the shallow Reyðarártindur Pluton, southeast Iceland. Primarily, the exposed pluton is constructed of a single rock unit, the Main Granite (69.9–77.7 wt.% SiO_2). Two further units are locally exposed as enclaves at the base of the exposure, the Granite Enclaves (67.4–70.2 wt.% SiO_2), and the Quartz Monzonite Enclaves (61.8–67.3 wt.% SiO_2). Geochemically, the units are related and were likely derived from the same source reservoir. In 3D, the pluton has a shape characterized by flat roof segments that are vertically offset and a volume of >2.5 km^3. The pluton roof is intruded by dikes from the pluton, and in two locations displays depressions associated with large dikes. Within these particular dikes the rock is partially to wholly tuffisitic, and rock compositions range from quartz monzonite to granite. We interpret these zones as eruption-feeding conduits from the pluton. A lack of cooling contacts throughout the pluton indicates rapid magma emplacement and a thermal model calculates the top 75 m would have rheologically locked up within 1,000 years. Hence, we argue that the Reyðarártindur Pluton was an ephemeral part of the wider plumbing system that feeds a volcano, and that timeframes from emplacement to eruption were rapid.

Plain Language Summary Scientists who monitor active volcanoes are interested in the pathways that magma takes on its journey through the crust to eruption. They use this information to aid in forecasting eruptions. Specifically, in Iceland it is known that magma often moves from chambers deep in the crust (>20 km) to shallow levels (<5 km) where the magma is stored for a time before it erupts (or does not erupt). Because scientists cannot physically "observe" active magma chambers in the crust, we turn to older, now fossil magma chambers, to examine what processes occurred during their construction. In this paper, we examined a shallow fossil magma chamber in Iceland and used geological mapping and geochemical analysis to reconstruct its history. We found that it has a "castle-like" shape with a minimum volume of 2.5 km^3, and was assembled in pulses of magma over a rapid timeframe. The magmas are silicic in composition, which is important from an eruption hazard perspective because silicic magmas have the potential to cause larger, explosive, eruptions. We also found evidence that the chamber erupted from at least two locations, and used a cooling model to determine that it could have been active for up to 1,000 years.

Key Points:

- The pluton was constructed in batches from silicic magmas that were all sourced from the same underlying reservoir
- Silicic magma injection may have been a trigger for eruption-feeding conduits in the roof
- The pluton was rapidly assembled and had a maximum eruptible lifetime of around 1,000 years

Supporting Information:

Supporting Information may be found in the online version of this article.

Correspondence to:

E. L. Rhodes and S. Burchardt,
emma.rhodes@geo.uu.se;
steffi.burchardt@geo.uu.se

Citation:

Rhodes, E. L., Barker, A. K., Burchardt, S., Hieronymus, C. F., Rousku, S. N., McGarvie, D. W., et al. (2021). Rapid assembly and eruption of a shallow silicic magma reservoir, Reyðarártindur Pluton, Southeast Iceland. *Geochemistry, Geophysics, Geosystems*, *22*, e2021GC009999. https://doi.org/10.1029/2021GC009999

Received 28 JUN 2021
Accepted 23 OCT 2021

Author Contributions:

Conceptualization: E. L. Rhodes, S. Burchardt
Data curation: T. Mattsson, T. Schmiedel, E. Ronchin
Formal analysis: E. L. Rhodes, C. F. Hieronymus, S. N. Rousku
Funding acquisition: S. Burchardt
Investigation: E. L. Rhodes, S. N. Rousku, T. Schmiedel, E. Ronchin, T. Witcher

1. Introduction

1.1. Context of Study

The dynamics of silicic magma assembly prior to eruption are of high interest for eruption forecasting, particularly because of the potential for silicic magma to cause larger, explosive eruptions (Thordarson & Larsen, 2007). Knowledge of the geometry, timescales and emplacement mechanisms of magma reservoirs aid in interpreting precursory signals (geophysical, geodetic, gas emissions etc.) to volcanic eruptions and therefore improve eruption forecasting and risk mitigation (Marti & Folch, 2005; National Academies of

Methodology: E. L. Rhodes, S. Burchardt, C. F. Hieronymus, S. N. Rousku
Project Administration: S. Burchardt
Software: C. F. Hieronymus
Supervision: S. Burchardt, D. W. McGarvie
Writing – original draft: E. L. Rhodes
Writing – review & editing: E. L. Rhodes, S. Burchardt, D. W. McGarvie, T. Mattsson, T. Schmiedel, E. Ronchin, T. Witcher

Sciences Engineering and Medicine, 2017). Moreover, the study of solidified and exposed volcanic plumbing systems provide information on the structure and dynamics of magma emplacement through the use of structural geological, petrological, and geochronological tools.

Generally, all these studies highlight that volcanic plumbing systems most likely exist in the form of uneruptible crystal mushes with melt pockets during most of their lifetime (e.g., Bachmann & Bergantz, 2004; Cashman et al., 2017; Edmonds et al., 2019). This "mush paradigm" entails that the eruption of considerable volumes of silicic magma requires relatively high rates of magma supply to fuel silicic magma production and the remobilization of the crystal mush (e.g., Annen, 2009; Bachmann & Bergantz, 2006; Cashman & Blundy, 2013; Edmonds et al., 2019; Huber et al., 2010; Sparks et al., 2019). However, the formation, role, and longevity of high-melt-fraction silicic magma bodies in the shallow crust immediately prior to eruptions remain enigmatic (cf. Edmonds et al., 2019; Glazner, 2021). In particular, the example of Krafla highlights that larger rhyolitic magma reservoirs may potentially form without easily detectable geophysical signals (cf. Rooyakkers et al., 2021).

Here, we use the Reyðarártindur Pluton as a case study to explore how silicic magma is assembled prior to eruption, as well as how magma from a shallow magma reservoir is supplied to surface eruptions. To do this, we first use mapping and 3D reconstruction to characterize the volume, shape and structure of the now solidified magmatic body. Second, we apply whole rock and feldspar geochemistry to derive the relationship between the different intrusive units. Third, we analyze structural features within the pluton roof and present evidence for eruption from the pluton. Lastly, we use a thermal model to determine the longevity of eruptible magma within the pluton. From our results, we aim to contribute to the understanding of the assembly of shallow silicic plumbing systems, as well as their eruptive potential and longevity.

1.2. Geological Setting

Iceland's highly abundant volcanism is interpreted to result from the interaction of the Iceland mantle plume with the Mid-Atlantic Ridge (Thordarson & Larsen, 2007). Volcanism in Iceland is centered along (a) rift zones reflecting the current on-land spreading location of the Mid-Atlantic Ridge, which produce magmas of tholeiite compositions, and (b) flank or off-rift zones, which are defined by a lack of rifting and by the production of magmas with alkaline compositions (Figure 1; Jakobsson, 1972; Jónasson, 2007; Thordarson & Hoskuldsson, 2008). The volcanism can further be segregated into discrete volcanic systems. A typical volcanic system comprises an elongate fissure swarm, with fissures aligned parallel to the spreading axis, and a central volcano (Figure 1a; Sæmundsson, 1979). The central volcano is considered the core hub for volcanic activity, containing a shallow magmatic plumbing system, and importantly is the main point of eruption for silicic volcanic rocks (Askew et al., 2020; Sæmundsson, 1979; Thordarson & Hoskuldsson, 2008; Thordarson & Larsen, 2007; Walker, 1966).

In Iceland, silicic rocks are generated by both (a) fractional crystallization, and (b) the partial melting of hydrothermally altered basaltic crust and older silicic volcanic rocks by the intrusion of hot basaltic magma (Banik et al., 2018; Jónasson, 2007; Padilla et al., 2016; Schattel et al., 2014; Sigurdsson & Sparks, 1981). Subsequently, the silicic magma may be transported via dikes and stored at shallow depths prior to eruption (e.g., Eyjafjallajökull: Keiding & Sigmarsson, 2012; and Krafla: Saubin et al., 2021). Such shallow-level silicic magma reservoirs may be several kilometers in diameter, such as evident from Krafla (Árnadóttir et al., 1998; Friðleifsson et al., 2014; Gasperikova et al., 2015; Kennedy et al., 2018) and exposed plutons in the eroded parts of Iceland (Blake, 1966; Burchardt et al., 2012; Furman et al., 1992; Walker, 1966).

The Reyðarártindur pluton is one of four km-sized silicic plutons exposed in the Neogene basaltic lava pile of Southeast Iceland (Figure 1b). It is exposed along the south and eastern sides of Reyðarártindur Peak, its namesake, as well as in the valleys associated with the Reyðará and Karlsá Rivers. Notably, it contains an exceptionally well-exposed stretch of the Reyðará River with magmatic enclaves (Figure 2). Apart from its appearance on maps and recent zircon dating, little research has been undertaken on the Reyðarártindur pluton (Gale et al., 1966; Padilla, 2015; Twomey et al., 2020; Walker, 1964). The depth of emplacement was likely around 1–2 km (Blake, 1966; Walker, 1960), and zircon dating gives crystallization ages of 7.30 ± 0.06 Ma (Padilla, 2015) and 7.40 ± 0.02 to 7.41 ± 0.04 Ma (Twomey et al., 2020). Since the plutonic complexes of Southeast Iceland are regarded the shallow crustal cores of Neogene central volcanoes

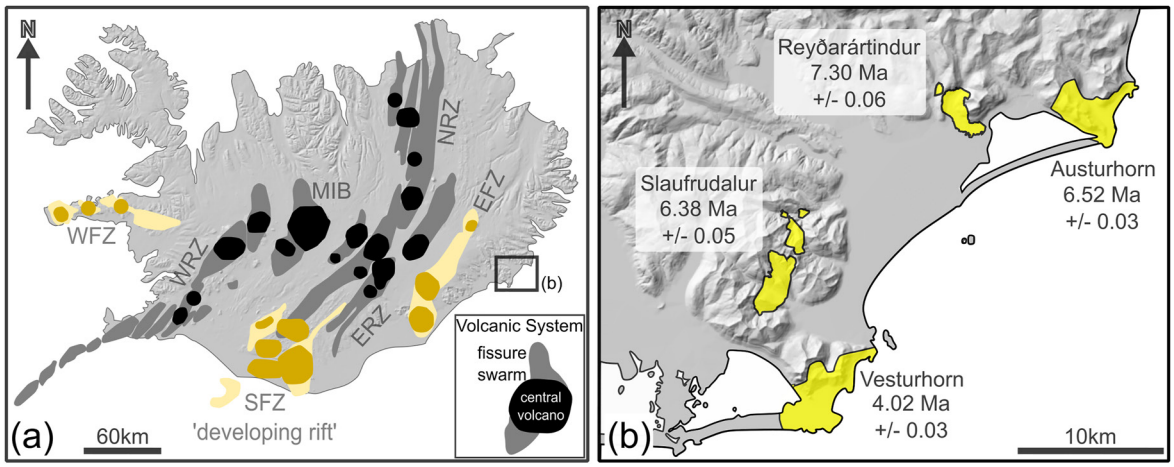

Figure 1. (a) Simplified map of Iceland showing the active volcanic systems (<0.8 Ma) after Jóhannesson and Sæmundsson (2009). A volcanic system is defined as containing a fissure swarm (yellow/gray), a central volcano (black/dark yellow), or both. On this map, the volcanic systems are divided by color into rift zones (gray/black), and flank zones (yellow/dark yellow). The rift zones are divided into the western (WRZ), eastern (ERZ), northern (NRZ), and mid Icelandic belt (MIB) rift zones. Likewise, the different flank zones are referred to as the western (WFZ), eastern (EFZ) and southern flank zone or "developing rift" (SFZ). Black box indicates location of (b). (b) Map of the Southeast Iceland Intrusive Suite (SIIS). The outline for Slaufrudalur is based on Burchardt et al. (2012), for Austurhorn is based on Blake (1966), for Vesturhorn is based on Jóhannesson and Sæmundsson (2014), and Reyðarártindur from the mapping conducted during this study. Ages are from Padilla (2015). Digital elevation models and coastline outline for both maps were downloaded from Landmælingar Íslands (www.lmi.is).

(Furman et al., 1992), studying Reyðarártindur provides insight into the processes of silicic magma reservoir emplacement and eruption, with analogies to the modern-day volcanoes.

1.3. Terminology

In this study we use the term *enclave* to describe an inclusion of one rock unit inside a host rock unit, in 2D exposure (as per Paterson et al., 2004). An enclave may be round, that is, pillow shaped, or angular with straight edges.

In addition, the literature often separates mingling from mixing (or hybridization). Hybridization between mingling magmas is a commonly documented phenomena worldwide (i.e., Morgavi et al., 2017). For this study, we define mingling and hybridization as per Morgavi et al. (2017) where *mingling* is the term for mechanical mixing without obvious chemical exchange, and where *hybridization* requires obvious chemical exchange and diffusion. When we describe two or more rock units in contact with each other as enclaves, we use the term *mingling*, unless we have evidence for chemical exchange, that is, *hybridization*. Hybridization could be determined by geochemical analysis, for example.

1.4. Nomenclature

We have named the rock units based on (a) their composition in the Total Alkali and Silica (TAS) naming scheme (LeBas et al., 1986), and (b) a descriptive word which describes the unit's location or form within the pluton. For example, the Main Granite is the primary rock unit exposed in the pluton and it is granitic in composition, and the Quartz Monzonite Enclaves are quartz monzonite in composition and exposed as enclaves. In addition, we refer to the Reyðarártindur body simply as a pluton, in reference to the broad definition of a pluton as a body of intrusive rock. We are aware that it could be termed a sub-volcanic complex, due to its shallow depth (<2 km) (i.e., Magee et al., 2013), or a laccolith, if it was determined that space for the magma intrusion was created by uplifting the overlying host rock (cf. Mattsson et al., 2018).

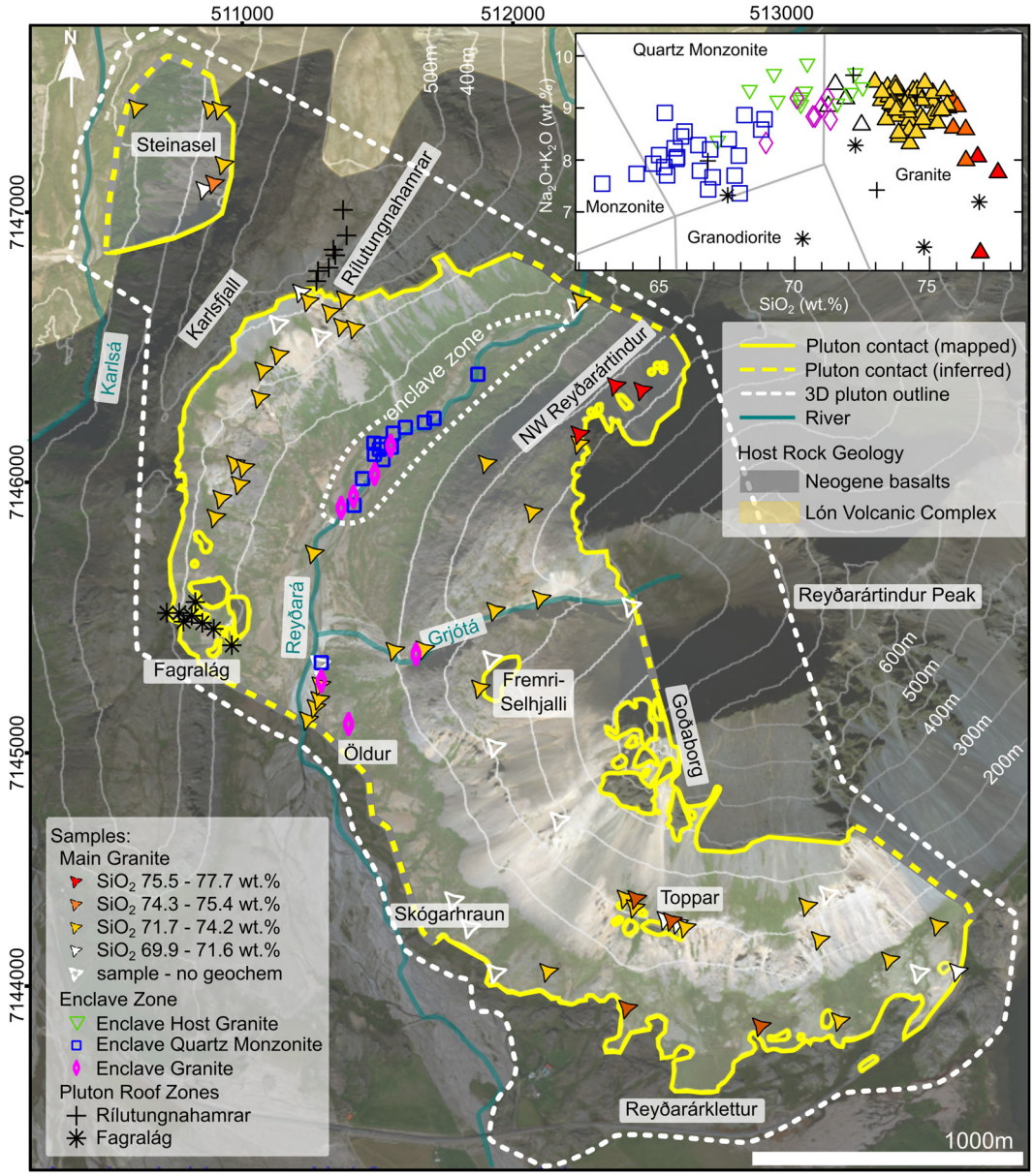

Figure 2. Map of the Reyðarártindur Pluton, with localities mentioned in the text. Locality names have been adapted from the Landmælingar Íslands map viewer (www.lmi.is). The letter á at the end of a name stands for river. Therefore, Reyðará denotes Reyðará River. The yellow border indicates the pluton outcrop extents and the dashed white line indicates the 3D extent of the pluton projected to the surface (see model in Figure 4). Aerial photo from Bing Maps. Coordinate system WGS 84/UTM 28N. Top right inset: Total Alkali and Silica geochemical classification for the Reyðarártindur Pluton (LeBas et al., 1986). The Reyðarártindur suite ranges from monzonite to granite in composition.

2. Materials and Methods

2.1. Contact Mapping

The detailed geological mapping presented here (Figure 2) builds on reconnaissance-level maps by Walker (1964), Gale et al. (1966) and Padilla (2015). The pluton was mapped during three field campaigns, the first time in August 2018 and again in June and August 2019. Where possible, contacts were mapped from ground reconnaissance with hand-held GPS and complemented by mapping on aerial photographs (Bing Maps). Unmanned Aerial Vehicle (UAV) "drone" imagery filled in the gaps where access was restricted, and where the aerial photographs are unclear (i.e., due to shadows). Strike and dip measurements of the contact

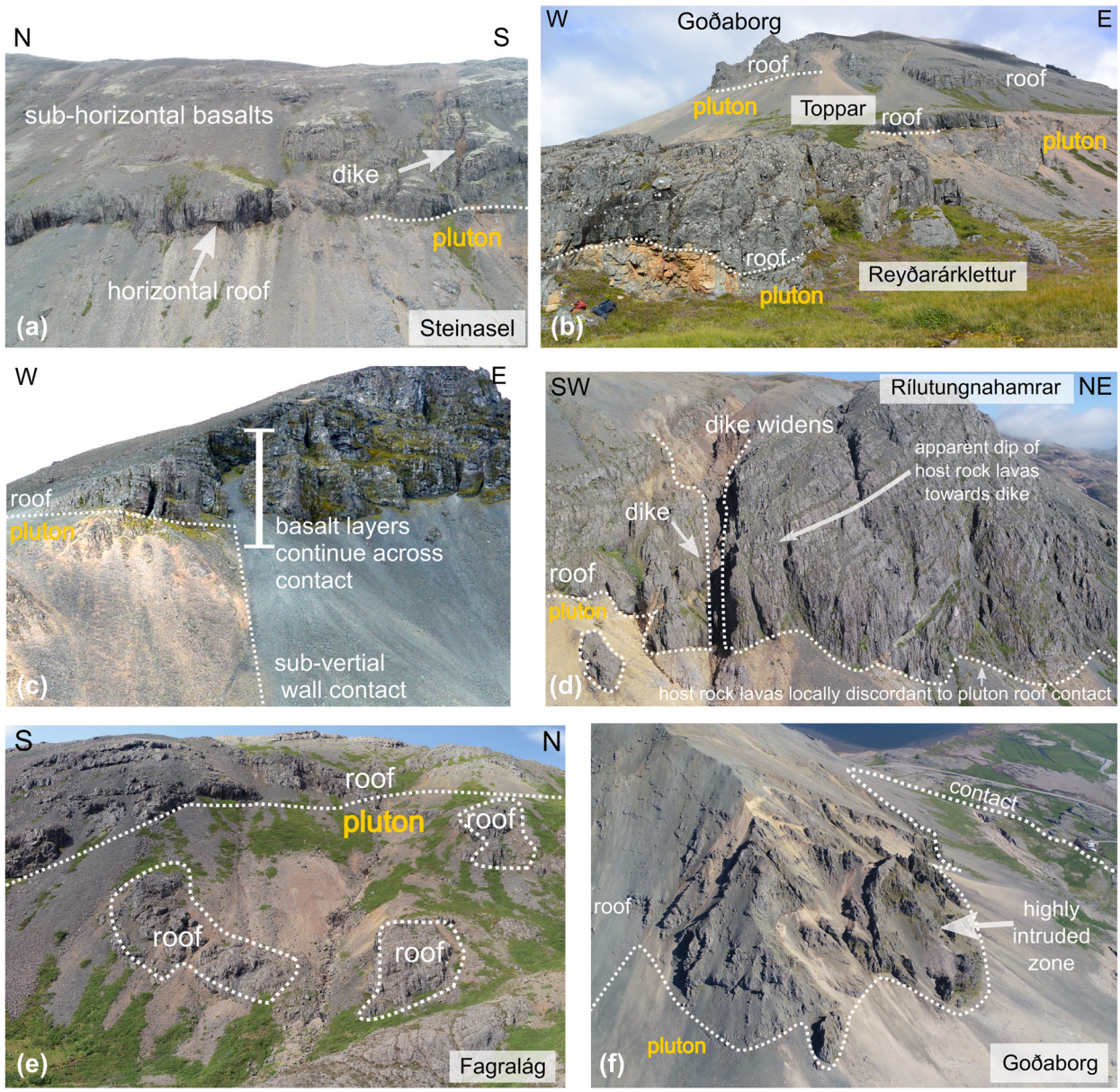

Figure 3. Photos of key features and locations. (a) A typical horizontal roof contact with conformable basalt lava flows. (b) View north from Reyðarárklettur to Toppar and Goðaborg, demonstrating adjacent roof exposures with vertical offsets. (c) Example of a sub-vertical wall contact where the conformable basalts continue across the contact at the top. Unfortunately, the wall sides are covered by scree. (d) Unmanned Aerial Vehicle (UAV) photo of the Rílutungnahamrar locality. Here you can see where the dyke widens to ca. 30 m at the top. Also notable is the apparent dip of the host rock lavas towards the dyke. (e) UAV photo of the Fagralág locality, where the downfaulted roof is exposed in several patches. (f) UAV photo looking down on Goðaborg, where the roof is heavily intruded by dykes from Reyðarártindur pluton.

were taken in the field where feasible. All data was imported into the MOVE™ 2019 software (https://www.petex.com/products/move-suite/), and the contact was drawn in 3D view, overlain on a 2 m spatial resolution digital elevation model (Arctic DEM).

2.2. 3D Model

The MOVE™ software was also used for 3D reconstruction of the Reyðarártindur Pluton. The roof surface was created using Delaunay Triangulation from 46 cross sections of the roof oriented N-S and 22 oriented NW-SE (300–120°). As most roof exposures are flat-lying (Figure 3a), we assumed that the roof in

unexposed and eroded locations is flat. When we encountered roof outcrops that are exposed at different elevations, we inferred a step, that is, a steeply-dipping fault, between them (i.e., between Goðaborg and Toppar, and Goðaborg and Fremri-Selhjalli; Figure 2). The floor of the pluton is not exposed, therefore a minimum lower elevation of −50 meters above sea level (m asl) was specified. This value was selected as part of the sub-horizontal pluton roof is exposed at sea level, and it is therefore reasonable to assume that the pluton extends at least 50 m below. We note that the calculated volume is therefore a minima, and this is taken into consideration in the discussion. A detailed list of inferences is provided in Text S1 in Supporting Information S1.

2.3. Petrology and Geochemistry

One hundred and seventy five samples of at least 10 cm^3 were obtained from outcrops across the pluton, with higher sampling density in the Reyðará River area where there was a wide range of lithologies (Figure 2). Thin sections slabs were cut at Uppsala University, and then sent for thin section preparation at the Slovak Academy of Sciences, where they were polished using a diamond paste. Modal abundances of the mineral phases were visually estimated from the thin sections. Samples for geochemical analysis were cut at Uppsala University and cleaned via scrubbing in water with a brush and soaking in an ultrasonic bath. At least 100 g of each sample was then crushed in a steel jaw crusher and milled to a fine-grained powder in a tungsten carbide mill at the Natural History Museum (Naturhistoriska Riksmuseet), Stockholm. Approximately 20 g of each sample was sent to ALS geochemistry in Vancouver, Canada where major and trace element geochemistry was performed. Whole rock major oxide geochemistry was processed via fused disc X-Ray Fluorescence (XRF), and Loss On Ignition (LOI) by furnace or thermogravimetric analysis. For trace element geochemistry, sample powders (0.100 g) were added to a lithium metaborate/lithium tetraborate flux, mixed well, and fused in a furnace at 1025°C. The resulting melt was then cooled and dissolved in an acid mixture containing nitric, hydrochloric, and hydrofluoric acids. This solution was then analyzed by inductively coupled plasma-mass spectrometry. Analytical precision for the major oxides is 3% of the value measured for Al_2O_3, BaO, CaO, Fe_2O_3, MgO, and SiO_2; 5% for BaO, Cr_2O_3, K_2O, MnO, Na_2O_3 and TiO_2; 10% for SO_3 and SrO; and Total 2%. Analytical precision for the trace elements is 10% of the measured concentration.

Some results returned with LOI >2 wt.%, namely six enclave samples from the Reyðará River zone and all samples from the Fagralág and Rílutungnahamrar zones (see Section 3.4). The enclave samples showed no deviation from the lower LOI samples when LOI was plotted against the major oxides, in particular Na and K, and therefore the samples were considered suitable to be included in the study. For the Fagralág and Rílutungnahamrar samples there was no low LOI equivalent to compare them with and therefore they are included in the study, but the high LOI (2–4.5 wt.%) was considered when interpreting the data.

2.4. River Enclave Statistics

Statistical results of enclave size and distribution were extracted from drone photographs of the Reyðará River. Overlapping photos of the Reyðará River were acquired using a DJI Phantom 4 Pro UAV with a photo resolution of 5472 × 3648 pixels. Three ground control points were taken along the transect using a Garmin GPSMap Handheld GPS system. Additionally, to ground-truth the scale, the horizontal scale of identifiable features were measured at several locations along the transect. Three drone images of ca. 40 m long sections of the river were selected based on (a) spacing and (b) feasibility for analysis. The enclaves were manually mapped in Inkscape. Areas that were obscured by gravel or unfeasible for analysis were removed from the data set. The images were then imported into ImageJ (Schneider et al., 2012), and the IJBlob plugin (Wagner & Lipinski, 2013) was used to quantify enclave size and host-enclave proportion. Orientation of the long axis of enclaves was quantified using the measure tool in ImageJ, which provides the orientation of the long axis of an enclave (ferret diameter) counterclockwise from the positive *x*-axis. These results were then corrected to north and imported into Stereonet 10 (Cardozo & Allmendinger, 2013) for the construction of rose diagrams. In order to avoid scatter from the smaller, more equant enclaves, only the largest 300 of a total 1,424 enclaves by area for the northernmost image, and the largest 200 of a total 432 enclaves for the second analyzed image were imported into Stereonet 10 for Rose diagram construction. In the other two

images, the enclaves were either too small for feasible analysis, or the enclaves were too few and large for statistical relevance.

2.5. Electron Microprobe Analysis

Mineral chemistry of 14 selected feldspar crystals, plus three elemental maps, were acquired using the field emission source JEOL JXA-8530F Hyperprobe at the Department of Earth Sciences, Uppsala University, Sweden. For the spot analysis profiles, the run conditions were 15 keV accelerating voltage and 10 nA probe current, with a defocused beam of 5 microns. Elemental maps were analyzed using the wavelength dispersive system (WDS) with 100 ms dwell times at 4 nA and 15 keV. The pixel size is 1.0 μm. Analytical standards for the JEOL JXA-8530F Hyperprobe are reported in full in Barker et al. (2015). In summary, the analytical uncertainties for major oxides which typically have concentrations >10 wt.% such as SiO_2 and Al_2O_3 are ≤1.5% s.d.. Major oxides with typical concentrations of 5–10 wt.% such as Na_2O and CaO have analytical uncertainties of ≤2.2% s.d.. When the elemental or oxide concentration is in the range of 2–5 wt.%, the uncertainties are ≤4.5% s.d., which is the case for most of the K_2O in albitic feldspars. For the remaining elements and major oxides that have concentrations below 1.5 wt.%, notably F, Cl and TiO_2, analytical uncertainties are ≤10% s.d..

2.6. Thermal Cooling Model

A 3D cooling model was computed in COMSOL Multiphysics using the Finite Element Method. The model is purely thermal and does not take dynamic effects into account, such as convective motion of the melt or hydrothermal circulation in the host rock. To integrate the latent heat of crystallization, we use a piecewise linear discretization of the degree of melting provided by the thermodynamic code R-MELTS as reported by Cooper and Kent (2014). While the total latent heat released during solidification is the same as for a linear model, the bulk of solidification and hence of latent heat release occurs over a rather narrow temperature range from about 770°C to 720°C. The pluton is modeled using an ellipse with the closest possible parameters to the exposed pluton of $x = 4{,}700$ m, $y = 1{,}700$ m and $z = 600$ m. While the horizontal extent of the physical pluton is well constrained from field observations, the vertical extent is relatively poorly constrained. We thus additionally test a magma reservoir model with double the vertical semi-axis ($z = 1{,}200$ m). An initial temperature of 900°C was defined based on the temperature of the rhyolite body intersected during the IDDP drilling program at Krafla (Saubin et al., 2021). The model domain is a rectangular box with horizontal dimensions $L_x = 15$ km and $L_y = 10$ km and height $L_z = 5$ km. The box is sufficiently large such that, over the timescales of the model, only a negligible temperature change (less than 0.01°C) occurs at the boundaries due to the heat conducted away from the magma chamber. The top and bottom boundaries of the box are set to fixed temperature values of $T = 0$°C and $T = 700$°C, respectively, and the temperature throughout the box is initialized to a linear geotherm with a gradient of $dT/dz = 140$°C/km. Our main focus of interest is the timescale over which eruptible melt is available in the magma chamber. A dacitic magma mush reaches a critical crystallinity of 40%–60% at a temperature of about 750°C (Cooper & Kent, 2014). At this temperature, the effective viscosity of the mush rapidly increases and the mush thus becomes largely immobile and hence impossible to erupt. Expanded methods, model parameters, and equations are available in Text S2, Figures S6 and S7 and Table S1 in Supporting Information S1.

3. Results

3.1. Shape of the Reyðarártindur Pluton

The host rock for the Reyðarártindur pluton comprises of (a) Neogene basalt lava flows and (b) in the north-west, some intercalated rhyolite lavas from the Lón Volcanic Complex (Figure 2). The roof basalts to the Reyðarártindur pluton are mostly sub-horizontal (±10°) and the roof contacts are sharp and usually concordant with the roof basalts (Figure 3a). The basaltic lavas at the contact have a distinct dark and shiny appearance that extends several meters from the contact, and are heavily intruded by granitic veins and dikes that originate from the pluton. The dikes are 0.5–10 m wide and can be densely spaced (ca. 5 m) or widely spaced (ca. 50 m), depending on the location. Veins are typically 0.5–3 cm wide and follow regular joint structures in the roof with spacings of <3 m. Adjacent roof exposures occur with vertical offsets of

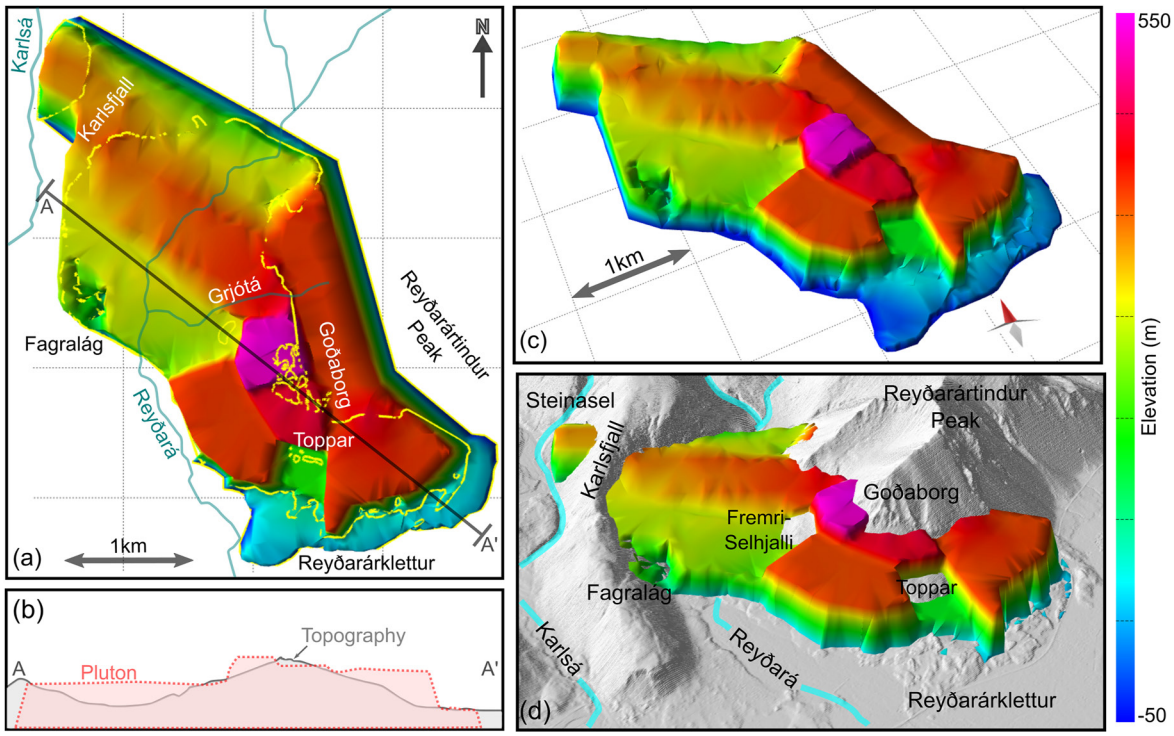

Figure 4. 3D reconstruction of the Reyðarártindur pluton to −50 m asl. The calculated volume of the reconstruction is 2.5 km^3. (a) Birds eye view. Contact (yellow) and names of areas from Figure 2 for reference. (b) Cross section of A–A' (see (a) for location). The topographical trace through the cross section is marked in gray, and the projected pluton outline in red. (c) View looking north-east and down onto the pluton. (d) The same view and scale as (c), with additional digital elevation model.

up to 200 m, creating both structural highs, for example, at Goðaborg, and lows, for example, at Toppar and Fremri-Selhjalli (Figure 3b). Sparse outcrops and the contact suggest that the pluton wall contacts are sub-vertical and discordant to the host lavas (Figure 3c). Hence, in 3D the pluton is a complex angular rhomboid with a central ridge along the long axis and a high at Goðaborg (Figure 4). The long axis (trend 320°) is 4.72 km long and the short axis (trend 65°) is 1.65 km wide, giving a surface area of ca. 8 km^2 in map view. A minimum volume of 2.5 km^3 was calculated down to −50 m asl. There are three notable exceptions to the conformable roof structure: Rílutungnahamrar, Fagralág, and Goðaborg, which are described and discussed further in Section 3.4 below.

3.2. Description and Distribution of Rock Units in the Pluton

3.2.1. The Main Granite

A macroscopically homogenous porphyritic granophyric microgranite (hereafter called the Main Granite) comprises the bulk of the exposed pluton (>90%; Figure 2). In hand sample the Main Granite has a small grainsize (from ca. 1–3 mm) and varies in color from white to pink-beige on weathered surfaces and light to darker gray on fresh surfaces (Figure 5). Subhedral feldspar phenocrysts (3–5 mm) comprising <10% of the sample can be observed. Microscopic investigation reveals that feldspar (50–60 modal %) and quartz (35–45 modal %) dominate with variable amphibole (1–5 modal %) and minor opaque minerals (<5 modal %). The feldspars are turbid and sometimes zoned, and some display more acicular versus tabular shapes, especially closer to the roof contact. Granophyric to graphic intergrowths of quartz with alkali- and plagioclase feldspar dominate the groundmass (Figure 5 and Figure S1 in Supporting Information S1).

Although we define the Main Granite as one unit, some local outcrops suggest that it was emplaced as multiple smaller magma units, or batches. There are two notable zones which preserve mingling with/within the Main Granite. First, below the roof contacts of Toppar and Reyðarárklettur, there is mingling between the host Main Granite and another granite geochemically identical to the Main Granite (refer to Section 3.2

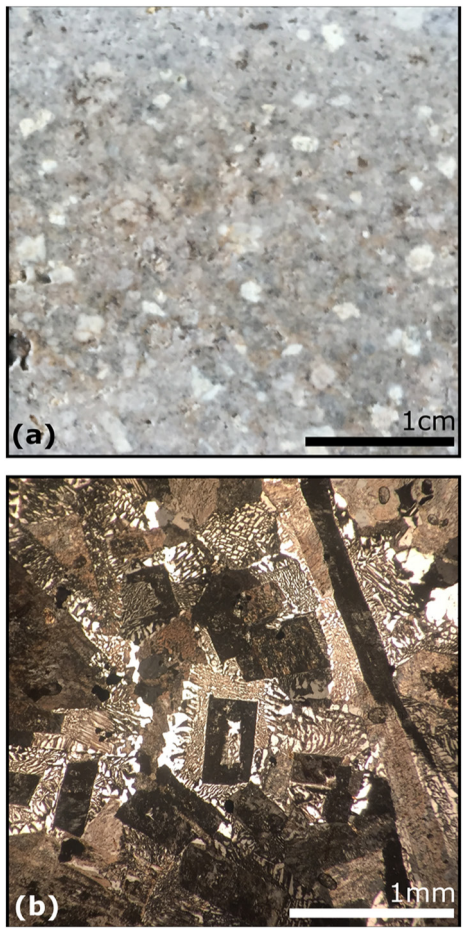

Figure 5. Representative photos of Main Granite in (a) hand sample and (b) thin section. In hand sample the plagioclase phenocrysts are white and the quartz-feldspar groundmass is gray. In thin section, quartz is white and the feldspar is altered to brown in color. Note the quartz-feldspar intergrowths (granophyric texture) that dominate the groundmass.

below). The second granite is finer grained and gray in color, with similar mineralogy to the Main Granite. Furthermore, internal cooling contacts between Main Granite batches are observed at two locations, both close to the pluton roof: one at Fremri-Selhjalli and the other at Steinasel. At the Fremri-Selhjall contact, we observed a chilled margin in the lower Main Granite unit. At Steinasel, the contact is marked by a structural change in jointing with a pervasively jointed lower unit and a sparsely jointed upper unit. A chilled margin in the lower unit accompanies the structural contact. Both contacts are local phenomena and cannot be traced further than 10's of meters. Photos are provided in Figure S2 in Supporting Information S1. A summary of key information on the Main Granite is presented in Table 1.

3.2.2. The Enclave Host Granite

An exceptionally well-exposed stretch of the Reyðará River contains a 1.5 km long zone where the granitic host rock unit contains enclaves of two further rock units (Figure 6). In hand sample, the plutonic host rock surrounding the enclaves appears very similar to the Main Granite, as it is typically light gray in color with white feldspar phenocrysts (Figure 7). Its color does differ slightly with weathering, which turns surface colors ranging from beige to pinkish to purple. Texturally, the samples contain feldspar phenocrysts and a groundmass of subhedral turbid feldspars and anhedral quartz, with zones displaying granophyric texture (Figure 7). Feldspar is the most dominant mineral (40–50 modal %), followed by quartz (20–40 modal %), amphibole (5–10 modal %) and opaque minerals (5 modal %). The maximum grain size is 2–3 mm, and hence can be classified as a microgranite. Notably, there is a gradational contact between the Main Granite and the host granite unit surrounding the enclaves and the host unit often contains tiny (<5 mm) inclusions of the enclaves (Figure 7). We term this rock unit the Enclave Host Granite and consider its relationship to the Main Granite in the discussion. A summary of the Enclave Host Granite is presented in Table 1.

3.2.3. Quartz Monzonite Enclaves and Granite Enclaves

We term the enclave rock units hosted within the Enclave Host Granite the Quartz Monzonite Enclaves and Granite Enclaves (Figures 2 and 6). The enclaves range from mm-size to 15 meters, are angular to rounded, and the proportion of enclaves to host in the analyzed Reyðará River segments ranges from 54% to 82% (Figure 6). Both enclave lithologies can be found throughout the central river zone, but the Granite Enclaves extend further south to Öldur, and higher up into the Grjótá River (Figure 2). The Quartz Monzonite Enclaves are more prevalent and can be much larger in size (Granite Enclaves were only observed to be <1 m diameter). However, the Granite Enclaves sometimes have shapes that are more irregular, preserving folding and stretching (Figure S3 in Supporting Information S1).

Veins of the Enclave Host Granite commonly separate larger enclaves into smaller, angular blocks, which grade into jigsaw-fit patterns as the pieces separate further. The northernmost river segment displayed in Figure 6 shows a preferred W-E orientation of enclaves, but this was the only segment where this was observed. The enclave margins do not display evidence of either chilled margins or broken crystals, although there is sometimes a decrease in crystal size in either the host or the enclave towards the contact (Figure S3 in Supporting Information S1). Some enclave margins are well defined, sharp, and jagged with larger enclave crystals protruding into the host. Other margins are more diffuse with a mix of host and enclave

Table 1
Summary of Key Properties of Rock Units in the Reyðarártindur Pluton

	Location	Geochemistry	Features
Main Granite	All pluton excluding the Reyðará River zone.	69.9–77.7 wt.% SiO_2 (near roof) but most samples plot in the narrower 71.7–74.3 wt.% SiO_2 range.	A macroscopically homogenous feldspar-phyric granophyre. Some mingling exposed near roof outcrops.
Quartz Monzonite Enclaves	Enclaves within Reyðará River zone.	61.8 to 67.3 wt.% SiO_2	Phaneritic with distinct amphibole needles. Largest and dominant enclaves in the Reyðará River zone.
Granite Enclaves	Enclaves within Reyðará River zone.	67.4 to 70.2 wt.% SiO_2	Dark gray and fine-grained with small amphibole laths. Smaller and less volumetrically dominant enclaves. Often have more irregular enclave shapes, preserving folding and stretching.
Enclave Host Granite	Host rock unit that surrounds the enclaves in the Reyðará River. Gradational contact with the Main Granite.	66.7 to 71.3 wt.% SiO_2	Feldspar-phyric granophyre, similar in appearance to Main Granite.
Intrusive features in the pluton roof	Fagralág, Rílutungnahamrar and most likely Goðaborg.	65.1 to 75.6 wt.% SiO_2. Some deviations in major oxides (Ca, Na, K, Al), but trace elements plot on same trends as the other rock units.	Subsidence in the overlying basalt roof rocks surrounds these intrusive features. Intrusive rock contains small to extensive tuffisites.

crystals at the boundary. At these enclave-host margins, it is common to see crystals from an enclave in the host or vice versa.

The mineral assemblage of the Quartz Monzonite is dominated by plagioclase and alkali feldspar (60–80 modal %), amphibole (15–20 modal %), quartz (10–20 modal %) and opaque minerals (2–10 modal %, Figure 7). In hand sample, this lithology shows a variety of crystal sizes (1–10 mm), modal proportion, and color. The finer-grained samples appear dark gray and aphanitic, and the coarser-grained samples are black and white, and phaneritic with distinct amphibole needles (Figure 7). Although the samples look equigranular at hand sample scale, microscopically, the samples can be seen to consist of 70%–80% of phenocrysts of feldspar and amphibole with an interstitial groundmass. All mineral types are present in the groundmass, and quartz sometimes displays graphic intergrowth with alkali and plagioclase feldspar. The feldspar phenocrysts are tabular to lath-shaped, euhedral to subhedral, and often zoned. Nearly all feldspars are turbid, especially around the zoned crystal edges. Amphibole phenocrysts are acicular with the long axis ranging from 1 to 15 mm. Opaque minerals are commonly associated with the amphibole.

The Granite Enclave unit is distinguished by its gray color and fine grain size (<2 mm) in hand sample (Figure 7). The mineral assemblage of the Granite Enclaves is dominated by feldspar (50–60 modal %) and quartz (35–40 modal %), with additional amphibole (5–10 modal %) and opaque minerals (<5 modal %). Microscopically, the Granite Enclaves vary in texture, and range from samples which contain a groundmass of acicular feldspars, to samples which are equigranular with tabular feldspars (Figure 7). Quartz is more equant, anhedral, and smaller than the feldspars. Amphibole is acicular and commonly altered to chlorite. Opaque minerals are associated with all mineral phases. Rare larger euhedral plagioclase phenocrysts of up to 5 mm can be found. A summary of key information on the Quartz Monzonite Enclaves and Granite Enclaves is presented in Table 1.

3.3. Whole Rock Geochemistry

The suite of rocks from the pluton (including the Main Granite, Enclave Host Granite and Enclaves) plots together and displays a trend from monzonite to granite (Figure 2). In Harker diagrams, the different lithologies plot together as one large suite, which range from the Quartz Monzonite Enclaves with the lowest

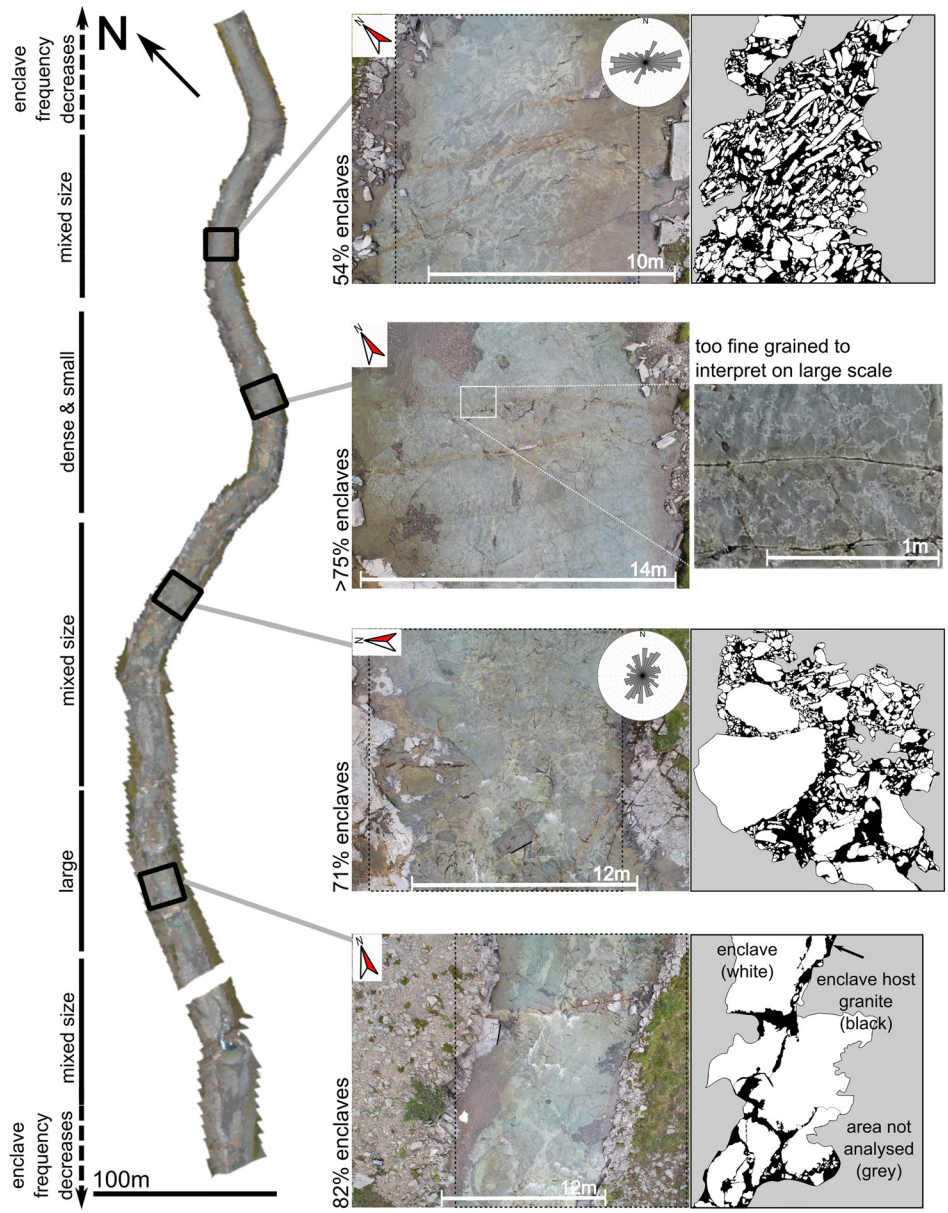

Figure 6. Mosaic and representative Unmanned Aerial Vehicle photographs of the Reyðará River stream bed. Corresponding traced enclave distribution (white) for three of the four sections are shown in the right column, and rose diagrams of enclave orientation for two of the four. The traced images have irregular edges as tracing was limited to areas with good resolution. To the left of the mosaic, an interpretation of enclave size and distribution along the river length is provided.

silica values, to the Main Granite with the highest (Figure 8). Specifically, the silica range of the Main Granite is 69.9–77.7 wt.%, and the Granite Enclaves and Enclave Host Granite have similar silica contents of 66.7–71.3 and 67.4 to 70.2 wt.%, respectively. The Quartz Monzonite Enclaves have silica contents of 61.8–67.3 wt.%. A summary of the silica contents of the different lithologies is given in Table 1.

The silica content of the Main Granite shows some trends based on location within the pluton. Samples from the majority of the pluton plot in the narrower 71.7 to 74.2 wt.% silica range and samples near the roof contacts (i.e., Toppar, Reyðarárklettur, NW Reyðarártindur and Steinasel; Figures 2 and 8) span a wider range of silica compositions from 69.9 to 77.6 wt.%. Furthermore, samples with the highest silica content of 75.5–77.7 wt.% were all restricted to the northwestern Reyðarártindur slopes. Notably, most and least

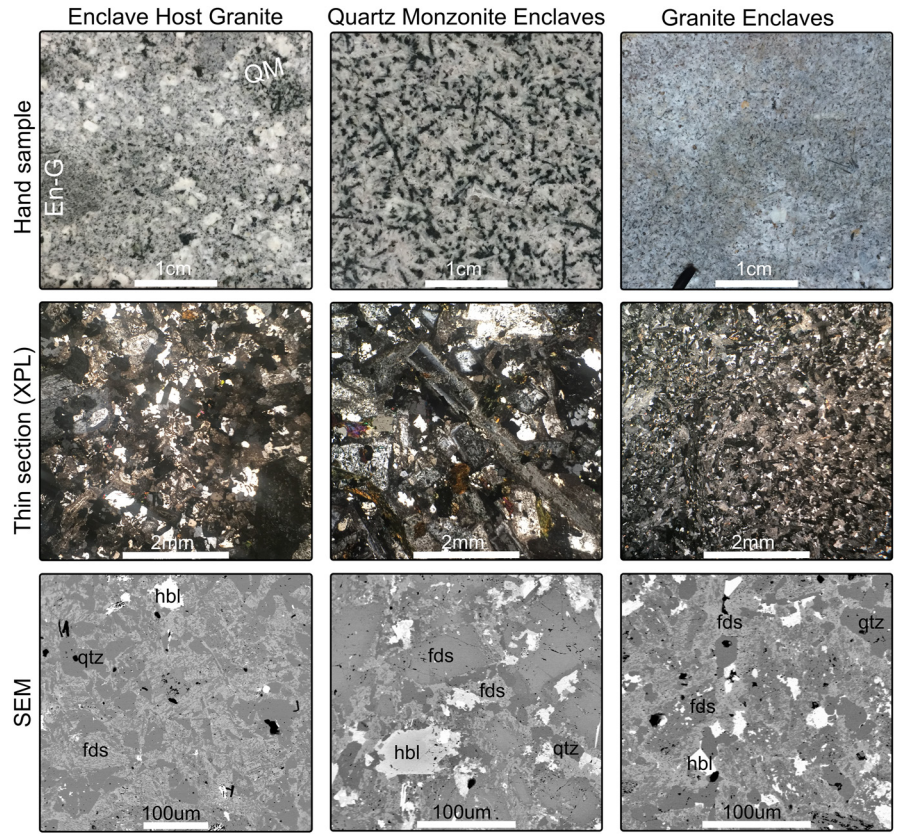

Figure 7. Representative hand sample photos (upper), pictomicrographs (in XPL, middle) and back scatter electron images (lower) of the Enclave Host Granite, Quartz Monzonite Enclaves and Granite Enclaves. The hand sample photo of the Enclave Host Granite contains small enclaves of both the Quartz Monzonite (QM) and Granite (En-G) lithologies. Note that the microscopic textures of the Granite Enclaves vary from sample to sample.

evolved samples could not be connected to unique characteristic textures, despite the mingling interactions exposed at Toppar and Reyðarárklettur.

Most major oxides in the Reyðarártindur suite define curvilinear trends in Harker diagrams (Figure 8). Concentrations of TiO_2, Fe_2O_3, and CaO decrease to almost zero with increasing SiO_2 and have well-defined compositional trends. The oxides Na_2O and Al_2O_3 have flat trends against SiO_2 in the Quartz Monzonite enclaves and decrease above 68 wt.% SiO_2. K_2O is the only major oxide that does not have a simple curvilinear trend. Quartz Monzonite Enclave concentrations are constant at ca. 3 wt.% K_2O, whereas the Main Granite concentrations are constant at ca. 5 wt.% K_2O. These two fields are linked by the compositions of the Enclave Host Granite and the Granite Enclave samples.

Within the Main Granite, the higher-silica samples located at the roof contacts (>75 wt.% SiO_2) contain wider ranges of concentrations of some major oxides compared to the rest of the Main Granite (Figures 2 and 8). Specifically, they contain a wider K_2O range of 1–5 wt.% compared to ca. 5 wt.%, a wider Al_2O_3 range of 9–13 wt. % compared to ca. 13 wt.%, and to a lesser extent a wider range of Fe_2O_3 with 1.5–3 wt.% compared to ca. 1.5 wt.%. The same samples also extend up to CaO 4 wt.%, and MgO 0.3 wt.%. The concentrations of TiO_2 and Na_2O align with those of the Main Granite.

Compatible trace elements (Eu, Zr, Sr, and Hf) in the samples exhibit a negative trend with silica, and incompatible trace elements (Th, Nb, Rb and Ta) present positive trends with silica (Figure 9). Barium exhibits a negative trend with silica within the Main Granite field from 700 to 250 ppm, and flat trends within the Quartz Monzonite Enclave and Granite Enclave groups at concentrations of 400–520 ppm and 450–550 ppm, respectively. Within the Enclave Host Granite, Ba has concentrations of up to 300 ppm higher than the other units, at 580–800 ppm. Additionally, there is an Enclave Host Granite sample (at SiO_2 67

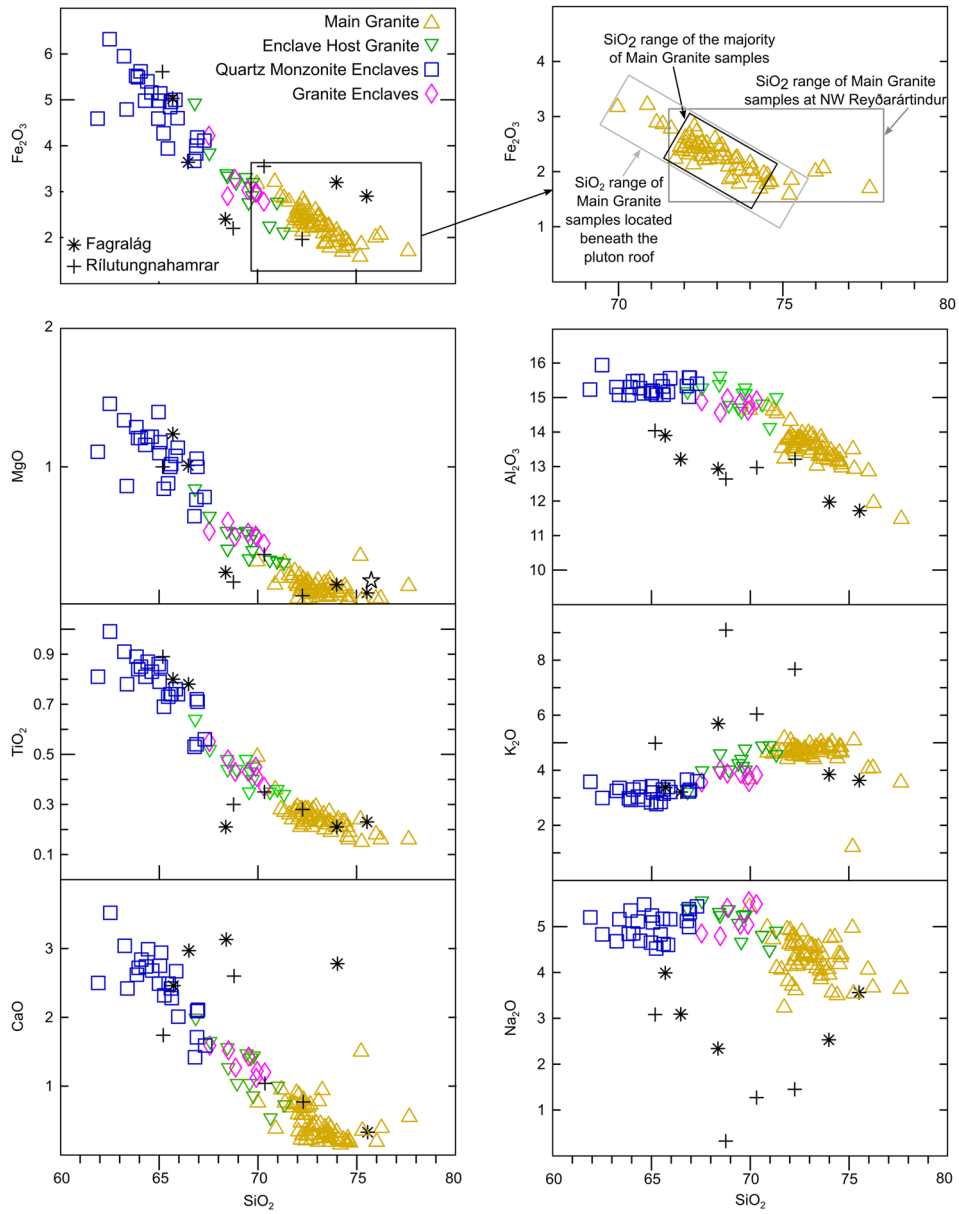

Figure 8. Selected Harker diagrams for the Reyðarártindur Pluton. All values in wt.%. The top right diagram is an enlargement of the Main Granite suite for Fe_2O_3, with the spatial distribution of higher and lower SiO_2 values noted. See Figure 2 for spatial distribution of SiO_2.

wt.%) that contains anomalously high trace element concentrations of Ta, Th, Nb, Hf and Zr. We consider this sample to be anomalously enriched, possibly via zircon or other crystals hosting many trace elements. The remaining quantified trace elements exhibit flat or highly scattered trends with SiO_2 (Nd, Ga, Lu, Tm, Yb La, Cs, Dy, Gd, Ho, Pr, Sn, Tb and W).

Although the elements plot as a single suite on almost all major and trace element graphs, trace element ratio graphs display three separate trends for the Main Granite, Granite Enclaves, and Quartz Monzonite Enclaves (Figure 10). The K_2O/Nb ratios are similar, spanning from 0.09 to 0.13 for the Main Granite and Granite Enclaves and 0.07 to 0.13 for the Quartz Monzonite Enclaves. Zr/Nb ranges from 7 to 14 for the Main Granite, 15 to 25 for the Granite Enclaves and 17 to 28 for the Quartz Monzonite Enclaves (Figure 10a). They form three groups with positive trends between Zr/Nb and K_2O/Nb. The Enclave Host Granite plots scattered between the Enclave Granite and Main Granite suites, with a K_2O/Nb from 0.10 to 0.15 and a Zr/Nb

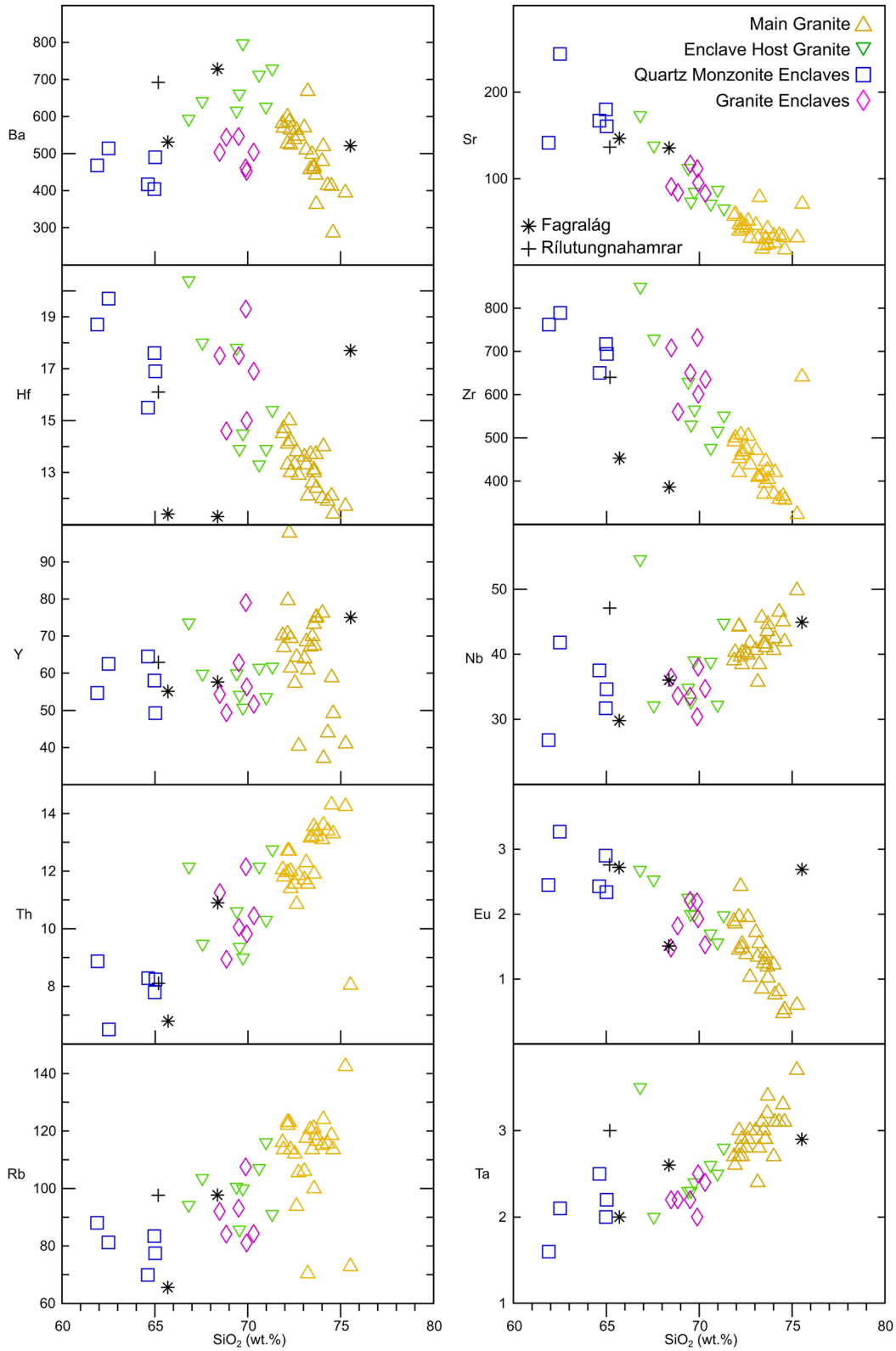

Figure 9. Selected whole rock trace element geochemistry for Reyðarártindur pluton. All trace element values in ppm.

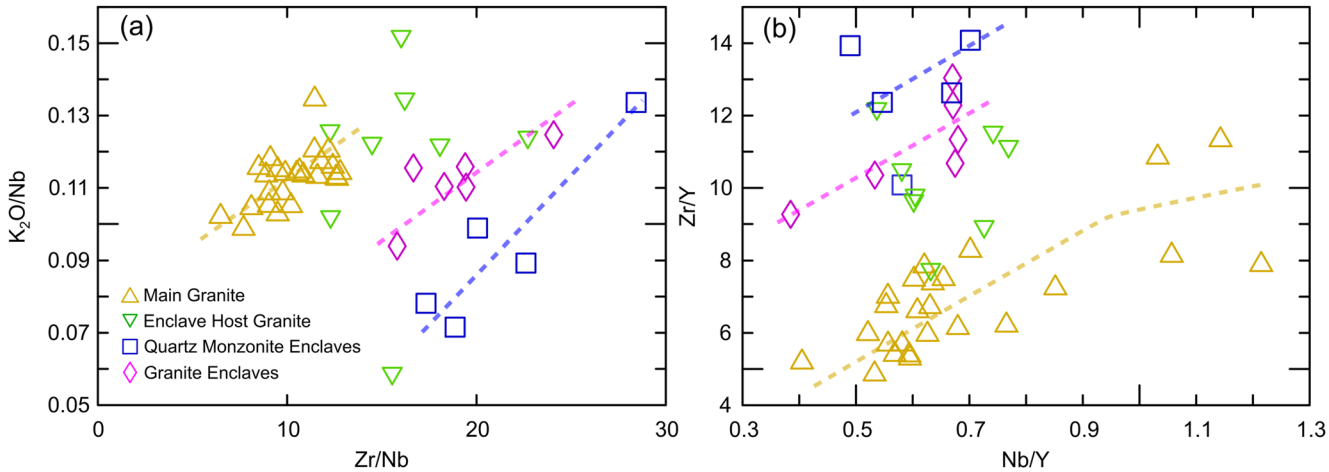

Figure 10. Selected element ratios (a) K_2O/Nb versus Zr/Nb, and (b) Zr/Y versus Nb/Y, displaying individual differentiation trends (indicated by dashed lines) within the Main Granite (yellow), Granite Enclaves (pink), and Quartz Monzonite Enclaves (blue). The Enclave Host Granite (green) spans a wider range between groups. Zr, Nb, and Y are in ppm. K_2O is in wt.%. Note the sample with the low K_2O/Nb is the probably enriched sample mentioned in the text.

from 12 to 24. Likewise, the Nb/Y ratios overlap, ranging from 0.4 to 0.7 for the Quartz Monzonite Enclaves and Granite Enclaves and an extended range from 0.4 to 1.2 for the Main Granite (Figure 10b). However, the groups are separated by, and positively correlated with Zr/Y. The Zr/Y ranges from 10 to 14 for the Quartz Monzonite Enclaves, 9 to 13 for the Granite Enclaves, and 4.5 to 11 for the Main Granite. The Enclave Host Granite has lower Nb/Y with a range of 0.5–0.8, but a larger Zr/Y range of 7–12, and does not define a linear trend parallel to those of the other groups. Instead, it plots scattered between all samples, but in particular the Enclave Granite and Main Granite suites.

3.4. Feldspar Chemistry

In the Main Granite, the three analyzed plagioclase phenocrysts were consistently andesine in composition ($An_{26–43}$), with two of the phenocrysts preserving a sharp step to $<An_{10}$ at the rim (i.e., sample KV6, Figure 11). Similarly, within the Quartz Monzonite Enclaves, the three analyzed plagioclase phenocrysts have consistent core compositions at the andesine/labradorite boundary of ca. An_{50}. The rims of these feldspars also preserve a step down to ca. An_{10} (i.e., sample R8, Figure 11).

Compositions of the feldspars within the Granite Enclaves are more heterogeneous, with both inverse and normal zoning, and different core compositions. For example, sample R2b (Figure 11) has an oligoclase core of $An_{14–23}$, and the outermost 100 μm to the rim has an increase in the average anorthite content with a range of $An_{19–30}$. In contrast, phenocryst R9_F1 (Figure 11) contains an andesine core with a linearly decreasing anorthite content from An_{42} to An_{30}. The outermost 300 μm decreases in average anorthite content towards An_{10} at the outermost rim, but contains increases and decreases of anorthite by up to An_{18} between sampling points (15 μm). A second phenocryst from the same sample showed similar results. Plagioclase crystals in the Enclave Host Granite display two populations of core compositions: the first has a labradorite composition of $An_{45–60}$, and the second has an oligoclase composition of $An_{18–30}$. The labradorite samples display steady core compositions and normal zoning to An_{10} over a distance of 150–300 μm at the rims. In contrast, the oligoclase samples display little to no zoning. Additional crystal profiles provided in Figures S4 and S5 in Supporting Information S1.

3.5. Anomalous Zones in the Pluton Roof

3.5.1. Rílutungnahamrar

At this site, there is a prominent NNW-striking dike approximately 10 m wide rising from the pluton and cutting through a 50 m thick section of the roof basalts (Figures 2 and 3d). To the northeast of the dike, the exposed pluton roof contact is locally discordant to the basalt layering, and the westward dipping lavas are

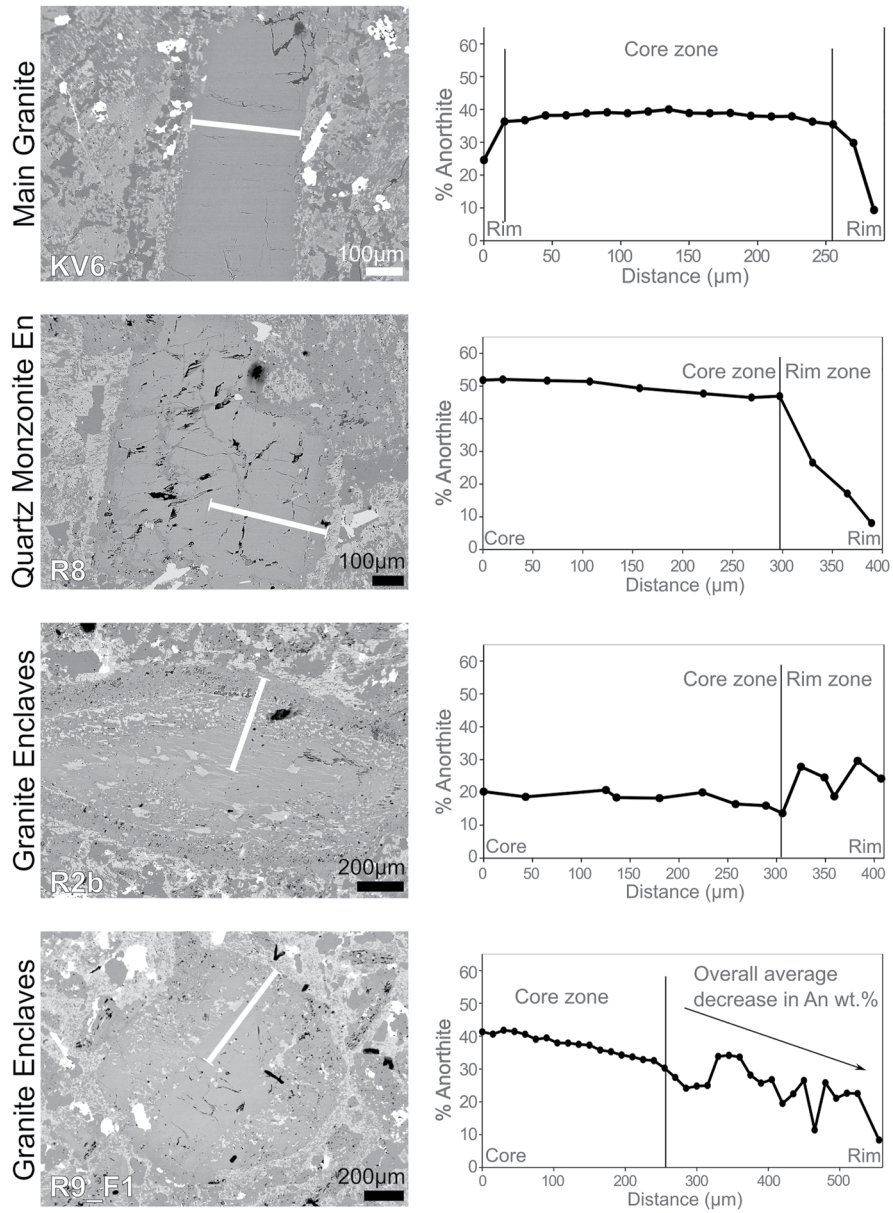

Figure 11. Selected back scatter electron images of feldspar crystals (left) and analyzed profiles (right) for the Main Granite, Quartz Monzonite Enclaves, and Granite Enclaves. Additional crystal profiles available in Figures S4 and S5 in Supporting Information S1.

crosscut by the pluton contact. The overall structure gives the appearance that the roof basalts have subsided towards the dike (Figure 3d). At the origin of the dike at the pluton-roof contact, coherent Main Granite was exposed within the dike, although a small zone of local brecciation of the Main Granite was also observable. At the highest exposed elevations, the dike widens to approximately 30 m. Here, the dike material is now wholly composed of veins of variably sintered fine grained pyroclastic material containing fragments of granophyre, stretched pumice and basaltic lithics (Figures 12a–12c). We refer to this material as a tuffisite, in the growing recognition that tuffisites can be dike-scale phenomena (cf. Schipper et al., 2021). The tuffisite samples collected vary in color, clast size, proportion and texture and veins can be centimeter to meter scale in thickness.

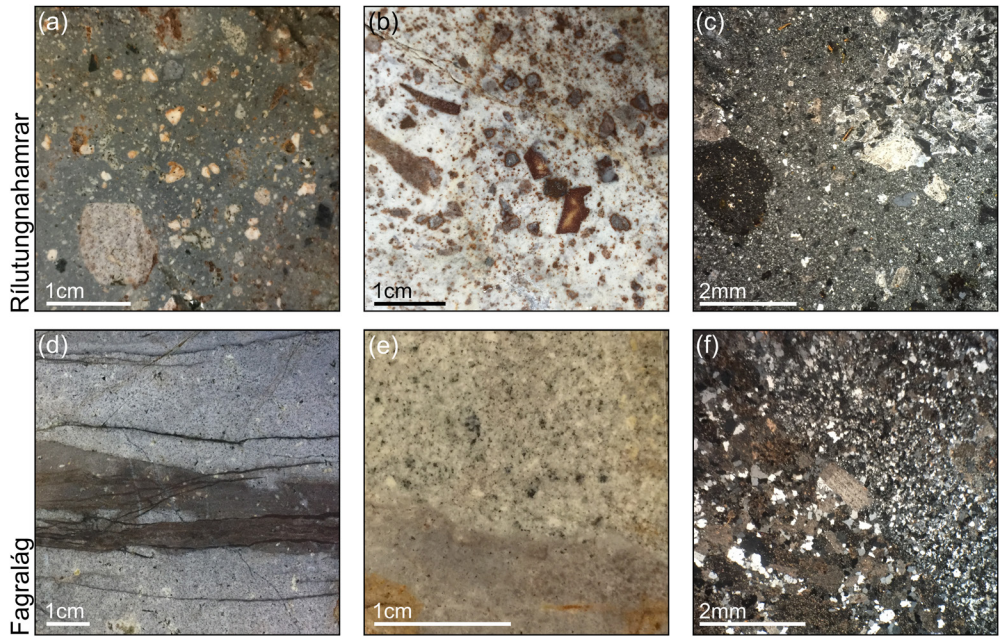

Figure 12. Photos and pictomicrographs of rock samples from Rílutungnahamrar and Fagralág. (a) and (b) are hand samples from Rílutungnahamrar displaying the diversity of the breccias exposed. (c) Pictomicrograph in CPL of Rílutungnahamrar breccia displaying textural diversity of clasts and fine grained matrix. (d) and (e) are hand samples from Fagralág, (d) shows multiple tuffisite veins cutting through a granite and (e) shows the contact between the Main Granite (upper) and a finer grained granite. (f) Pictomicrograph of contact between rock units at Fagralág. Note there is alteration visible in all of these samples, particularly in the clasts, which are changing to a burnt orange color in (a) and (b). Furthermore, the feldspars in all of these samples are altering to clays.

3.5.2. Fagralág

At this site, which coincides with a corner in the pluton walls, multiple separated blocks of the pluton roof (ca. 30 m^2 in size) are positioned at elevations up to 120 m lower than the adjacent roof contact (Figures 2 and 3e). Individual blocks are separated by several meter-wide dikes extending upwards from the pluton or by pluton exposures. Notably, no rock units from the Reyðarártindur suite have been found overlying the roof basalts of the blocks. Overall, the Fagralág area resembles a stepped depression in the pluton roof (Figure 4). Between and underneath the roof blocks, zones of intrusive rock are exposed which are connected to the Main Granite body. This intrusive rock is extremely heterogeneous, both macro- and microscopically, and contains different textured rocks mingled with one another (Figures 12d–12f). Some of the rocks exposed at Fagralág resemble the Main Granite, and some resemble the Quartz Monzonite and Granite Enclaves. All samples are altered, and in particular, the feldspar phenocrysts display high levels of alteration in thin section, and secondary calcite is visible in pores. Furthermore, local flow banding, local brecciation and tuffisites are observed within the samples.

3.5.3. Whole Rock Geochemistry of Rock Units at Fagralág and Rílutungnahamrar

We have grouped the areas of Fagralág and Rílutungnahamrar together in this section as the geochemical results show many similarities. Geochemical analysis was undertaken on tuffisites from the upper level of the dike at Rílutungnahamrar and from granitic rock units between and underneath roof blocks at Fagralág. Silica ranges widely in the samples from 65.1 to 75.6 wt.%, and range from quartz-monzonite and granodiorite to granite in a TAS classification system (Figure 2). The major oxides MgO, TiO_2, and Fe_2O_3, and most trace elements plot on the same trend as the pluton suite, however, oxides Al_2O_3, Na_2O and element Zr are depleted and oxide K_2O is either depleted or enriched (Figures 8 and 9). Ti and Hf are either depleted or similar to the pluton suite and CaO and Ba are either enriched or also similar.

3.5.4. Goðaborg

This site marks the highest exposures of the pluton, and is located along the main NW trending pluton axis (Figures 2 and 4). The topographical prominence and patchy appearance of Goðaborg make it an area of interest. Drone aerial photography shows that the outcrop comprises blocks of roof basalt separated by numerous granitic dikes connected to the pluton beneath (Figure 3f). Unfortunately, due to its inaccessibility, no samples were obtained from Goðaborg.

3.6. Thermal Cooling Model

Results from the thermal cooling model are presented in Figure 13. While the horizontal extent of the physical magma chamber is well constrained from field observations, the vertical extent is relatively poorly constrained, and thus we present two models (Figures 13a and 13b). Using the exposed thickness of the pluton of 600 m, the thermal model shows that the eruptible magma volume of 2.5 km^3 is halved by 1,000 years, and decreases to zero by 3,000 years. When the vertical extent of the modeled pluton is doubled to 1,200 m, resulting in a volume of ca. 5 km^3, the cooling timescale increases about three-fold. In this model, the eruptible magma volume is halved after 2,500 years, decreases to 1 km^3 by 5,000 years, and reaches zero by 9,000 years. Because we were interested in the cooling timeframes of different zones of the magma body, thermal profiles were measured 75 m inwards from the top, base, "short-end" and "long-end" contacts (Figures 13a and 13b). Results of the thermal profile 75 m below the top surface were similar between the two models, and rapidly cooled to rheological lockup at 700°C within ca. 1,000 years. The biggest difference between the two models was in the "short-end" and "long-end" profiles, which became less pronounced in the thicker model, significantly extending their cooling timeframes. The most central portion of the ellipsoid, with a shape that is more spherical, maintains the highest temperature for the longest time.

4. Discussion

Here, we first establish that the different intrusive rock units are geochemically related and ascertain that Reyðarártindur formed from magma batches sourced from the same source zone. Second, we propose a staggered emplacement model for the pluton, where the Main Granite is intruded first in small batches, which is followed by the Quartz Monzonite and Granite Enclaves. Some hybridization occurs locally between the Enclaves and the Main Granite. Third, we set out evidence that the anomalous zones in the pluton roof of Rílutungnahamrar, Fagralág and Goðaborg are in fact remnants of eruption-feeding conduits. Lastly, we use a thermal model to determine the longevity of eruptible magma within the pluton and possible timing of events. With this information, we argue that the Reyðarártindur Pluton was an ephemeral part of the wider plumbing system of a volcano, and that timeframes of formation to eruption were geologically rapid.

4.1. Magmatic System

4.1.1. Relationship of the Magmas—A Common Source Reservoir

Through geochemistry, we assess that the different intrusive rock units are geochemically related, and therefore likely originated from a common source reservoir. Although the rock units or parental magmas can be separated into four geochemically distinct units (Main Granite, Quartz Monzonite Enclaves, Granite Enclaves and Enclave Host Granite), the units plot together as a coherent suite on Harker diagrams (Figures 8 and 9). The coherence of the trends indicates the intrusive rock units are geochemically related, likely via differentiation by fractional crystallization of amphibole, feldspar(s), and oxides. We tested this using a least squares minimization, which solved the magma evolution by fractionation of 34% plagioclase feldspar, 7.7% hornblende, 2.7% biotite, 1.6% alkali feldspar, and 3.5% Fe-Ti oxides (sum of squares 0.3515). Furthermore, there is some diversity and differentiation between and within the Main Granite, Quartz Monzonite and Granite Enclave groups, which is highlighted on trace element ratio plots (Figure 10). This implies that although the rock units are related, and therefore likely originated from a common source reservoir, the magmas were separated in some manner to achieve diversity. Such a separate evolution of related magmas could occur within a stratified source reservoir, or discrete melt lenses within a mush zone, or perhaps even by extraction of melt at different times from a melt-mush reservoir (Bachmann & Bergantz, 2004;

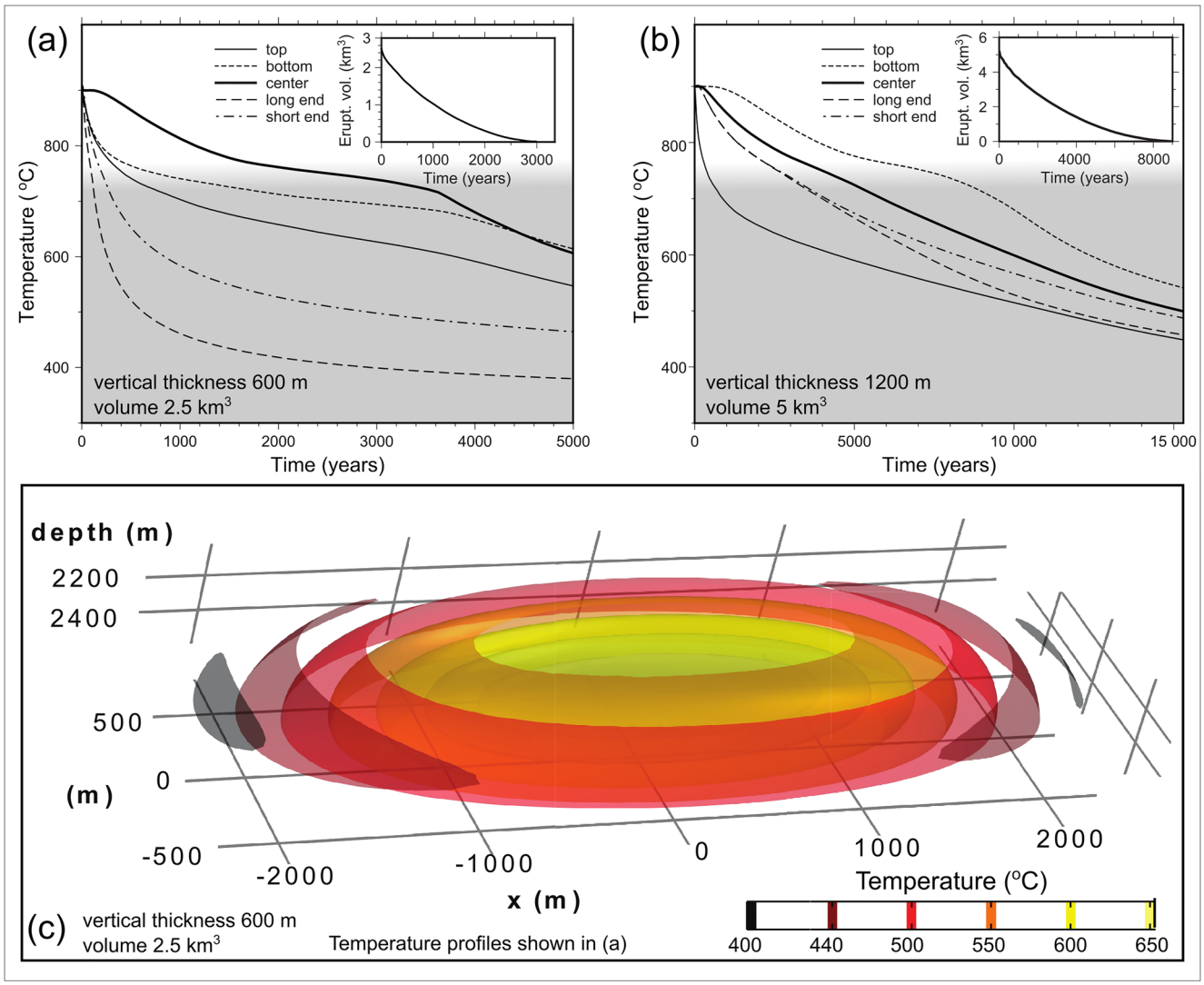

Figure 13. 3D pluton cooling model computed in COMSOL Multiphysics using the Finite Element Method. (a and b) Temperature of different parts of the pluton versus time. Model (a) is for the field constrained minimum vertical thickness of 600 m, and (b) is for double the minimum vertical thickness of 1,200 m. Profile points are taken 75 m inward from the edge and the gray area denotes the temperature of rheological "lock-up" (Cooper & Kent, 2014). Note, the "hump" around 4,000 years is due to the non-linearity of the melting model. Insets: Volume of eruptible magma in the magma reservoir as a function of time. Eruptible magma is defined as the volume of magma with a temperature at or greater than 750°C as per Cooper and Kent (2014). (c) Visualisation of the temperature field after 3,100 years for the model with 600 m vertical thickness. The temperature is displayed as a set of surfaces of constant temperature in order to give an optimal view of the geometry of the hottest portions of the pluton. In this model, the tapered ends of the elongate, ellipsoidal pluton have cooled fastest, while the most central portion of the ellipsoid, with a shape that is more spherical, has the highest temperature. This result illustrates that uncertainties in the details of the shape of the pluton, such as small protrusions or irregularities, have very little effect on the long-term cooling of the pluton.

Edmonds et al., 2019; Miller & Miller, 2002; Pistone et al., 2017; Scott et al., 2013). For a discussion of the possible tectonic framework during the emplacement of Reyðarártindur, the reader is referred to Text S3 in Supporting Information S1.

4.1.2. The Enclave Host Granite—Local Hybridization Between the Main Granite and the Enclaves

In hand sample, the host rock unit surrounding the enclaves appears almost identical to the Main Granite (albeit the small enclave inclusions), but it has a different geochemical signature (Figures 8–10). Additionally there is a gradational contact between the Main Granite and Enclave Host Granite. Generally, the Enclave Host Granite displays geochemical trends that plot on a straight line between the Main Granite and the Quartz Monzonite (with the exception of barium: Figures 8 and 9). A linear trend can indicate hybridization

between two end members, but can also be a result of fractional crystallization trends (e.g., Charreteur & Tegner, 2013; Jarvis et al., 2021; McGarvie et al., 1990; Scott et al., 2013; Weidendorfer et al., 2014). Notably, on the Harker Diagrams the Granite Enclaves also plot in a similar location to the Enclave Host Granite. However, the Enclave Host Granite differs from the Granite Enclaves in the trace element ratios K_2O/Nb versus Zr/Nb and Zr/Y versus Nb/Y (Figure 10). Here, the Enclave Host Granite samples lie scattered throughout the individual positive trends exhibited by the Granite Enclave, Quartz Monzonite Enclave and Main Granite groups. Such a trend supports hybridization between two or more end members, in this case the Main Granite and Quartz Monzonite and Granite Enclaves. Therefore, we consider that local hybridization occurred between the Main Granite and Enclaves, locally influencing the geochemical signature of the magma.

4.1.3. Feldspar Phenocrysts—Entrained During Melt Migration

Feldspar compositions record evidence of the magmatic conditions during their growth, and at Reyðarártindur, the feldspar phenocryst cores document growth in a more primitive melt than their rims. All the feldspars analyzed exhibit flat to gently normal-zoned core compositions (Figure 11), which are typical of closed system processes, where fractional crystallization and diffusion dominate (cf. e.g., Charreteur & Tegner, 2013; Costa et al., 2008; Streck, 2008; Weidendorfer et al., 2014). However, the rim zones of many of the feldspars display sharp changes in anorthite content. For example, in the Main Granite and Quartz Monzonite Enclaves there is a sharp decrease to albite composition (samples KV6 and R8, Figure 11), and in the Granite Enclaves there are sharp increases and decreases between sampling points (samples R2b, R9_F1, Figure 11). Sharp changes in anorthite content imply a change in pressure/temperature conditions or host melt composition, leading to disequilibrium between the crystal and melt (cf. e.g., Charreteur & Tegner, 2013; Costa et al., 2008; Streck, 2008; Weidendorfer et al., 2014; Morgavi et al., 2017). In other studies, crystals out of equilibrium with the melt have been interpreted as parts of the "mush system" that were entrained during ascent (Hansen & Grönvold, 2000; Passmore et al., 2012). Plagioclase crystals in particular are preferentially entrained in melts due to their relatively low density at high pressures (Flower, 1980; Hansen & Grönvold, 2000). Mush formation has been proposed under volcanoes of all compositions and settings in Iceland (Alfaro et al., 2007; Chekol et al., 2011; Flude et al., 2010; Gunnarsson et al., 1998; Hansen & Grönvold, 2000; Jónasson, 2007; Passmore et al., 2012). We therefore consider that the plagioclase phenocrysts were removed from a mush and entrained within a host melt of slightly different composition during melt migration.

4.2. Emplacement

4.2.1. Complex Pluton Shape—A Mixed Mode Emplacement Model

The emplacement of the Reyðarártindur pluton was structurally complex, as evidenced by the stepped 3D shape (Figure 4). The structure neither resembles the Slaufrudalur Pluton, where floor subsidence was the primary emplacement process, nor the Sandfell Laccolith, where roof uplift dominated (Burchardt et al., 2010, 2012; Mattsson et al., 2018). The faulted roof and undeformed walls preliminarily indicate a mixed mode emplacement model, which incorporates both roof deformation and floor subsidence. Such a model has for example been proposed for the Mourne Mountains Pluton, Northern Ireland (Mattsson et al., 2020).

4.2.2. Sequence of Magma Emplacement—A Model for Staggered Pluton Development

A schematic interpretation for pluton development that combines field, textural, and chemical observations of the Reyðarártindur Pluton is presented in Figure 14 and explained here.

1. The magma forming the Main Granite unit was emplaced first as it is exposed along the roof and wall contacts of the pluton. During the initial stages of intrusion, some Main Granite magma intruded in smaller batches (likely 100's of m^3). This is indicated by (a) the local contact-parallel chilled margins between granite rock units exposed near the roof (e.g., at Steinasel and Fremri-Selhjalli), (b) the granite-granite mingling between magmas preserved at Reyðarárklettur and Toppar, and (c) the wider compositional range of granites preserved near-roof zones of NW Reyðarártindur, Steinasel, Reyðarárklettur and Toppar (69.9–77.7 wt.% SiO_2, Figures 2 and 8).

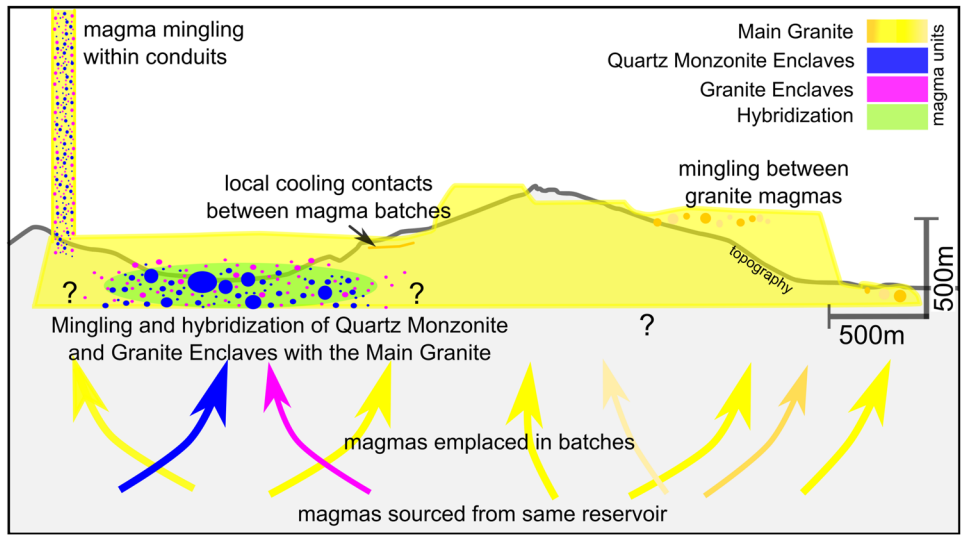

Figure 14. Schematic cross section of the Reyðarártindur pluton that combines structural, textural, and geochemical results.

2. Following the initial batch intrusion, the bulk of the Main Granite was either emplaced at a sustained rate, or magma batches were emplaced in an environment where the thermal contrast required for chilled margins was not achieved (Huppert & Sparks, 1989). In contrast to the near-roof zones, the smaller range of silica contents preserved within the bulk of the Main Granite unit either suggests less compositional heterogeneity of the magma during this stage (71.7–74.3 wt.%, Figures 2 and 8), or hybridization between the wider silica range of 69.9–77.7 wt.% (i.e., Charreteur & Tegner, 2013; McGarvie et al., 1990; Scott et al., 2013; Weidendorfer et al., 2014). Hybridization could be facilitated by longer timescales of cooling, and result in gradational chemical boundaries. Such longer cooling timescales could be caused by a higher intruding magma volume, or a shorter timeframe between magma batches, for example.
3. Following the Main Granite unit, less evolved granitic magma and quartz monzonite magma were emplaced into the pluton at/or below the level exposed in the Reyðará River. We neither see any evidence of the feeder system that led to enclave injection and dissemination, nor the order of enclave emplacement. However, the globular pillow-like shapes of the Quartz Monzonite and Granite Enclaves indicate that they were emplaced into a ductile Main Granite (Figure 6). Enclave formation could have occurred during emplacement by magma fingering owing to different rheological properties of the contrasting magmas, such as proposed for Austurhorn by Weidendorfer et al. (2014). The jigsaw fit and angular shape of some enclaves suggest enclaves were locally fractured by veins of the surrounding host magma (Figure 6). Fracturing likely occurred due to "back-veining" of the host through the enclaves (cf. Weidendorfer et al., 2014; Wiebe, 2016).
4. A degree of local hybridization between the Enclaves and the Main Granite occurred to produce the Enclave Host Granite unit (see Section 4.1.2).

4.3. Eruptive History

4.3.1. Rílutungnahamrar, Fagralág and Goðaborg—Remnants of Eruption Feeding Conduits

We consider the roof zones of Rílutungnahamrar, Fagralág and Goðaborg to be eruption feeding conduits, and we interpret that the roof and textural features in these areas are the result of magma erupting. If a dike reaches the surface to erupt it can cause a significant pressure decrease in the corresponding magma reservoir, triggering further evacuation of magma (Castro & Dingwell, 2009; Tarasewicz et al., 2012). At Reyðarártindur, we see local evidence of decompression in the fragmentation of the magma to form dike-scale tuffisites at Rílutungnahamrar and local tuffisites and breccias at Fagralág (Figure 12). If the magma supply from depth is not sufficient to keep the reservoir fully replenished, then deflation of the reservoir

and subsidence of the overlying host rock will occur (e.g., Sigmundsson et al., 2010). Subsidence of the host rock is likely to be most pronounced surrounding the eruption conduits (cf. Bertelsen et al., 2021). In the Reyðarártindur Pluton, we see evidence of host rock subsidence in the tilt of the roof rocks towards the dike at Rílutungnahamrar and the multiple subsided blocks at Fagralág (Figures 3d and 3e). Consequently, we consider the zones at Rílutungnahamrar, Fagralág, and most likely Goðaborg, to be remnants of eruption-forming conduits. Whether the eruption-forming conduits acted together or separately could not be determined. Furthermore, the host-rock subsidence implies that the eruptions were fed from the Reyðarártindur Pluton, and therefore the pluton must have been established prior to eruption.

4.3.2. Geochemical Variability of the Conduit Rocks—Multiple Magma Compositions Involved in the Eruptions

Despite variations in major oxide compositions, the trace elements show the conduit rock units were related to Reyðarártindur pluton rocks as they mostly plot on the same geochemical trends (Figures 8 and 9). Variations of major oxides Na, K and unusually also Ca and Al of the conduit samples from the Reyðarártindur pluton suite can be explained by hydrothermal alteration, as indicated by the high LOI for all the conduit samples (2–5 wt.%, higher than the standard LOI of <1.0 wt.% for the other rock units). LOI is often used as a proxy for hydrothermal alteration as hydrous minerals including many zeolites and carbon dioxide in calcite volatilize when heated to 1050°C during analysis (i.e., Franzson et al., 2008).

Hence, magmas sourced from, and spanning the entire range of compositions exposed at Reyðarártindur were involved in the eruptions (65–75 wt.% SiO_2, Figure 8). Notably, only magmas of silicic composition are exposed in the conduits and the entire pluton. This observation is in contrast to the common assumption that in Icelandic volcanoes, the interaction with basaltic magma is required to make silicic magma erupt. This assumption is based on numerous observations of basalts associated with silicic eruptions such as Eyjafjallajökull, Askja, Torfajökull, and Rauðafell, and composite dikes, such as at Streitishvarf (Charreteur & Tegner, 2013; Eriksson et al., 2011; McGarvie, 1984; Sigmundsson et al., 2010; Sigurdsson & Sparks, 1981). At Reyðarártindur, however, there is no evidence of basaltic magma interacting with the silicic ones. Instead, the wide compositional range of the conduit samples, corresponding to the different magma types observed in the pluton, suggest that the silicic magma injection events responsible for the magma mingling preserved in the pluton could have been an eruption trigger. Magma injection can contribute to eruption initiation through processes of heating and/or gas sparging, which can reduce the viscosity and increase the internal pressure of magma bodies (Bachmann & Bergantz, 2003, 2006; Murphy et al., 1998; Sparks et al., 1977). Additionally, we found no evidence of multiple intrusive rock units within dikes that were not associated with roof subsidence, supporting the interpretation that recharge of new magma into the pluton was required to trigger eruption. This may indicate that intrusion of the two enclave magmas into the core of the pluton (i.e., the Reyðará River) could have triggered eruption from the conduits described in this study. However, as there is no exposed or preserved spatial link between the Reyðará River Enclaves and the conduits, this course of events remains speculative.

4.4. Longevity and Eruption Potential of the Reyðarártindur Magma Reservoir

In the last decades geophysical, petrological, and geochronological evidence from active volcanic areas and exposed plutons has culminated in a paradigm shift. Volcanic plumbing systems are now viewed as a transcrustal column of crystal mush with a low amount of melt, except in local pockets (Cashman et al., 2017; Edmonds et al., 2019). For most of the lifetime of such a system, the crystal mush remains uneruptible, except when magma recharge leads to remobilization (Bachmann & Bergantz, 2003; Cooper & Kent, 2014). Still, instances where geothermal or scientific drilling has accidentally encountered magma in the shallow crust have highlighted that there may be reservoirs of high melt fractions in the shallow crust (Saubin et al., 2021; Zierenberg et al., 2013). Moreover, the observation of zoned megacrysts and crystal cargos with diverse crystallization histories are evidence for the existence of such reservoirs (Ginibre et al., 2002). However, the thermodynamic feasibility and longevity of such magma reservoirs are debated (Glazner, 2021).

Here, we propose that the Reyðarártindur Pluton was indeed emplaced as a high melt-fraction magma reservoir of considerable volume (at least 2.5 km^3) during geologically short time scales, based on three lines of evidence: (a) the internal contacts between units suggest magma emplacement into a ductile magma body

producing mingling between magma batches. (b) The only chilled margins within the pluton are of limited extent and restricted to near the roof, indicating they were produced during early magma batch intrusion. (c) The limited amount of hybridization between the Main Granite and the Enclaves suggest that prolonged timescales required for thorough hybridization were not met (cf. Petrelli et al., 2006). (d) No sharp contacts between the conduit rocks and the rest of the pluton occur, indicating that no crosscutting through a cooled pluton happened. (e) The same magmatic units that occur inside the conduits are present in the deepest exposed part of the pluton (the Reyðará River).

To arrive at a rough quantitative estimate of possible pluton longevity and eruption timeframes, we ran two thermal cooling models, one with the exposed thickness of the pluton (600 m) and one with double that thickness. The model calculates that the top 75 m of the pluton would have reached rheological lockup ca. 1,000 years after formation in both models, irrespective of pluton thickness (Figures 13a and 13b). To preserve the features listed above, a connection between mobile magma in the pluton core and the conduits in the roof was required, limiting the time from pluton emplacement to eruption to <1,000 years.

If the pluton was replenished by multiple magma injections at depth over longer time scales, the cooling duration could be extended (cf. Annen et al., 2015). However, the mingling of silicic magmas within the conduits suggest that recharge events favored eruption rather than growth. On the other hand, if hydrothermal circulation and magma convection in the reservoir were taken into account, as is not the case in the model, cooling timescales could be decreased by a factor of about 2–5 (cf. Andersen & Weis, 2020). Therefore, our model provides a conservative (i.e., maximum) cooling timeframe for the pluton. A short lifespan of the Reyðarártindur pluton as predicted in the model is also supported by zircon dating of samples across the pluton conducted by Twomey et al. (2020). The dating returned a narrow range of zircon crystallization ages of 7.40 ± 0.02, 7.41 ± 0.02 Ma, and 7.41 ± 0.04 Ma. All this evidence in the Reyðarártindur pluton points to rapid assembly prior to eruption, within cooling timeframes.

5. Conclusions and Implications for the Longevity and Eruption Potential of Silicic Magma Bodies

The results from this study suggest that silicic eruptions may be preceded by the rapid assembly of a shallow reservoir of high-melt fraction magma with a volume on the order of some km^3. The time from intrusion to eruption may be geologically short (within 1,000 years). Moreover, the existence of multiple conduits in the roof of the Reyðarártindur pluton suggests that such a reservoir may feed more than one eruption. Intrusion of basaltic magma may not be required to trigger an eruption, but notably, perhaps the intrusion of a new silicic magma can. A secondary implication of magma recharge triggering eruptions is that pluton growth may not be favored. Overall, the eruptive potential of a shallow reservoir such as Reyðarártindur is short-lived (1,000–5,000 years), much less than the duration of silicic magmatism in a typical Icelandic central volcano, or at other rhyolite-erupting volcanoes worldwide (in the order of hundreds of thousands to millions of years: Askew et al., 2020; Chambers et al., 2005; Flude et al., 2008; Hamilton et al., 1998; Singer et al., 2008; Storm et al., 2012). Additionally it supports the conclusion by Glazner (2021) that shallow, persistent magma bodies are not thermally viable. To conclude, our study of the Reyðarártindur pluton suggests that high-melt fraction magma bodies of considerable volume may assemble in the shallow crust above a deeper mush plumbing system and feed surface eruptions on geologically short time scales.

Data Availability Statement

Full whole rock geochemical data, EMP analysis tables and 3D model raw files for this study are loaded to Zenodo under the DOI of https://doi.org/10.5281/zenodo.4923170 (Rhodes et al., 2021).

Acknowledgments
This research was conducted as part of the first author's ongoing PhD research, funded by the Centre of Natural Hazards and Disaster Science (www.CNDS.se). First and foremost, the authors thank the owners of Reyðará Farm for allowing us to conduct fieldwork on their land. The authors also thank the owners of Dilksnes Guesthouse in Höfn for allowing us to sleep on their living room floor when we booked the wrong dates for accommodation. Additionally, the authors thank Per-Olof Persson for his assistance with the crushing and milling of samples at the Natural History Museum in Stockholm. Furthermore, the authors thank A. Padilla, an anonymous reviewer, and handing editor M. Edmonds for constructive comments that helped to improve this work. The study was financed by the Alice and Knut Wallenberg grant KAW 2017.0153, and The Royal Swedish Academy of Sciences grant GS2019-0024. Permission was granted for sampling from the Icelandic Institute of Natural History.

References

Alfaro, R., Brandsdóttir, B., Rowlands, D. P., White, R. S., & Gudmundsson, M. T. (2007). Structure of the Grímsvötn central volcano under the Vatnajökull icecap, Iceland. *Geophysical Journal International*, *168*(2), 863–876. https://doi.org/10.1111/j.1365-246X.2006.03238.x

Andersen, C., & Weis, P. (2020). Heat transfer from convecting magma reservoirs to hydrothermal fluid flow systems constrained by coupled numerical modeling. *Geophysical Research Letters*, *47*(23), e2020GL089463. https://doi.org/10.1029/2020GL089463

Annen, C. (2009). From plutons to magma chambers: Thermal constraints on the accumulation of eruptible silicic magma in the upper crust. *Earth and Planetary Science Letters*, *284*(3–4), 409–416. https://doi.org/10.1016/j.epsl.2009.05.006

Annen, C., Blundy, J. D., Leuthold, J., & Sparks, R. S. J. (2015). Construction and evolution of igneous bodies: Towards an integrated perspective of crustal magmatism. *Lithos*, *230*, 206–221. https://doi.org/10.1016/j.lithos.2015.05.008

Árnadóttir, T., Sigmundsson, F., & Delaney, P. T. (1998). Sources of crustal deformation associated with the Krafla, Iceland, eruption of September 1984. *Geophysical Research Letters*, *25*(7), 1043–1046. https://doi.org/10.1029/98GL50655

Askew, R. A., Thordarson, T., Gans, P., Thompson, J., & Danyushevsky, L. (2020). Temporal and spatial evolution of the Neogene age Breiðdalur central volcano through $^{39}Ar/^{40}Ar$ and U-Pb age determination. *Journal of Volcanology and Geothermal Research*, *404*, 107006. https://doi.org/10.1016/j.jvolgeores.2020.107006

Bachmann, O., & Bergantz, G. W. (2003). Rejuvenation of the Fish Canyon magma body: A window into the evolution of large-volume silicic magma systems. *Geology*, *31*(9), 789–792. https://doi.org/10.1130/G19764.1

Bachmann, O., & Bergantz, G. W. (2004). On the origin of crystal-poor rhyolites: Extracted from batholithic crystal mushes. *Journal of Petrology*, *45*(8), 1565–1582. https://doi.org/10.1093/petrology/egh019

Bachmann, O., & Bergantz, G. W. (2006). Gas percolation in upper-crustal silicic crystal mushes as a mechanism for upward heat advection and rejuvenation of near-solidus magma bodies. *Journal of Volcanology and Geothermal Research, 149*(1–2), 85–102. https://doi.org/10.1016/j.jvolgeores.2005.06.002

Banik, T. J., Miller, C. F., Fisher, C. M., Coble, M. A., & Vervoort, J. D. (2018). Magmatic-tectonic control on the generation of silicic magmas in Iceland: Constraints from Hafnarfjall-Skarðsheiði volcano. *Lithos*, *318–319*, 326–339. https://doi.org/10.1016/j.lithos.2018.08.022

Barker, A. K., Troll, V. R., Carracedo, J. C., & Nicholls, P. A. (2015). The magma plumbing system for the 1971 Teneguía eruption on La Palma, Canary Islands. *Contributions to Mineralogy and Petrology*, *170*(5–6), 1–21. https://doi.org/10.1007/s00410-015-1207-7

Bertelsen, H. S., Guldstrand, F., Sigmundsson, F., Pedersen, R., Mair, K., & Galland, O. (2021). Beyond elasticity: Are Coulomb properties of the Earth's crust important for volcano geodesy? *Journal of Volcanology and Geothermal Research*, *410*. https://doi.org/10.1016/j.jvolgeores.2020.107153

Blake, D. H. (1966). The net-veined complex of the Austurhorn Intrusion, Southeastern Iceland. *The Journal of Geology*, *74*(6), 891–907. https://doi.org/10.1086/627218

Burchardt, S., Tanner, D., & Krumbholz, M. (2012). The Slaufrudalur pluton, southeast Iceland-An example of shallow magma emplacement by coupled cauldron subsidence and magmatic stoping. *Bulletin of the Geological Society of America*, *124*(1–2), 213–227. https://doi.org/10.1130/B30430.1

Burchardt, S., Tanner, D. C., & Krumbholz, M. (2010). Mode of emplacement of the Slaufrudalur Pluton, Southeast Iceland inferred from three-dimensional GPS mapping and model building. *Tectonophysics*, *480*(1–4), 232–240. https://doi.org/10.1016/j.tecto.2009.10.010

Cardozo, N., & Allmendinger, R. W. (2013). Spherical projections with OSXStereonet. *Computers & Geosciences*, *51*, 193–205. https://doi.org/10.1016/j.cageo.2012.07.021

Cashman, K., & Blundy, J. (2013). Petrological cannibalism: The chemical and textural consequences of incremental magma body growth. *Contributions to Mineralogy and Petrology*, *166*(3), 703–729. https://doi.org/10.1007/s00410-013-0895-0

Cashman, K. V., Sparks, R. S. J., & Blundy, J. D. (2017). Vertically extensive and unstable magmatic systems: A unified view of igneous processes. *Science*, *355*(6331). https://doi.org/10.1126/science.aag3055

Castro, J. M., & Dingwell, D. B. (2009). Rapid ascent of rhyolitic magma at Chaitén volcano, Chile. *Nature*, *461*(7265), 780–783. https://doi.org/10.1038/nature08458

Chambers, L. M., Pringle, M. S., & Parrish, R. R. (2005). Rapid formation of the Small Isles Tertiary centre constrained by precise $^{40}Ar/^{39}Ar$ and U–Pb ages. *Lithos*, *79*(3–4), 367–384. https://doi.org/10.1016/j.lithos.2004.09.008

Charreteur, G., & Tegner, C. (2013). Magmatic emulsion texture formed by mixing during extrusion, Rauðafell composite complex, Breiðdalur volcano, eastern Iceland. *Bulletin of Volcanology*, *75*(6), 721. https://doi.org/10.1007/s00445-013-0721-6

Chekol, T. A., Kobayashi, K., Yokoyama, T., Sakaguchi, C., & Nakamura, E. (2011). Timescales of magma differentiation from basalt to andesite beneath Hekla Volcano, Iceland: Constraints from U-series disequilibria in lavas from the last quarter-millennium flows. *Geochimica et Cosmochimica Acta*, *75*(1), 256–283. https://doi.org/10.1016/j.gca.2010.10.001

Cooper, K. M., & Kent, A. J. R. (2014). Rapid remobilization of magmatic crystals kept in cold storage. *Nature*, *506*(7489), 480–483. https://doi.org/10.1038/nature12991

Costa, F., Dohmen, R., & Chakraborty, S. (2008). Time scales of magmatic processes from modeling the zoning patterns of crystals. *Reviews in Mineralogy and Geochemistry*, *69*, 545–594. https://doi.org/10.2138/rmg.2008.69.14

Edmonds, M., Cashman, K. V., Holness, M., & Jackson, M. (2019). Architecture and dynamics of magma reservoirs. Philosophical Transactions of the Royal Society A: *Mathematical, Physical and Engineering Sciences*, *377*(2139). https://doi.org/10.1098/rsta.2018.0298

Eriksson, P. I., Riishuus, M. S., Sigmundsson, F., & Elming, S.-Å. (2011). Magma flow directions inferred from field evidence and magnetic fabric studies of the Streitishvarf composite dike in east Iceland. *Journal of Volcanology and Geothermal Research*, *206*(1–2), 30–45. https://doi.org/10.1016/j.jvolgeores.2011.05.009

Flower, M. F. J. (1980). Accumulation of calcic plagioclase in ocean-ridge tholeiite: An indication of spreading rate? *Nature*, *287*(5782), 530–532. https://doi.org/10.1038/287530a0

Flude, S., Burgess, R., & McGarvie, D. W. (2008). Silicic volcanism at Ljósufjöll, Iceland: Insights into evolution and eruptive history from Ar–Ar dating. *Journal of Volcanology and Geothermal Research*, *169*, 154–175. https://doi.org/10.1016/j.jvolgeores.2007.08.019

Flude, S., McGarvie, D. W., Burgess, R., & Tindle, A. G. (2010). Rhyolites at Kerlingarfjöll, Iceland: The evolution and lifespan of silicic central volcanoes. *Bulletin of Volcanology*, *72*(5), 523–538. https://doi.org/10.1007/s00445-010-0344-0

Franzson, H., Zierenberg, R., & Schiffman, P. (2008). Chemical transport in geothermal systems in Iceland. *Journal of Volcanology and Geothermal Research*, *173*(3–4), 217–229. https://doi.org/10.1016/j.jvolgeores.2008.01.027

Friðleifsson, G. Ó., Ármannsson, H., Guðmundsson, Á., Árnason, K., Mortensen, A. K., Pálsson, B., & Einarsson, G. M. (2014). Site selection for the well IDDP-1 at Krafla. *Geothermics*, *49*, 9–15. https://doi.org/10.1016/j.geothermics.2013.06.001

Furman, T., Meyer, P. S., & Frey, F. (1992). Evolution of Icelandic central volcanoes: Evidence from the Austurhorn intrusion, southeastern Iceland. *Bulletin of Volcanology*, *55*(1–2), 45–62. https://doi.org/10.1007/BF00301119

Gale, N. H., Moorbath, S., Simons, J., & Walker, G. P. L. (1966). K-Ar ages of acid intrusive rocks from Iceland. *Earth and Planetary Science Letters*, *1*, 284–288.

Gasperikova, E., Rosenkjaer, G. K., Arnason, K., Newman, G. A., & Lindsey, N. J. (2015). Resistivity characterization of the Krafla and Hengill geothermal fields through 3D MT inverse modeling. *Geothermics*, *57*, 246–257. https://doi.org/10.1016/j.geothermics.2015.06.015

Ginibre, C., Wörner, G., & Kronz, A. (2002). Minor- and trace-element zoning in plagioclase: Implications for magma chamber processes at Parinacota volcano, northern Chile. *Contributions to Mineralogy and Petrology*, *143*(3), 300–315. https://doi.org/10.1007/s00410-002-0351-z

Glazner, A. F. (2021). Thermal constraints on the longevity, depth, and vertical extent of magmatic systems. *Geochemistry, Geophysics, Geosystems*, *22*(4), e2020GC009459. https://doi.org/10.1029/2020GC009459

Gunnarsson, B., Marsh, B. D., & Taylor, H. P. (1998). Generation of Icelandic rhyolites: Silicic lavas from the Torfajokull central volcano. *Journal of Volcanology and Geothermal Research*, *83*(1–2), 1–45. https://doi.org/10.1016/S0377-0273(98)00017-1

Hamilton, M. A., Pearson, D. G., Thompson, R. N., Kelley, S. P., & Emeleus, C. H. (1998). Rapid eruption of Skye lavas inferred from precise U–Pb and Ar–Ar dating of the Rum and Cuillin plutonic complexes. *Nature*, *394*(6690), 260–263. https://doi.org/10.1038/28361

Hansen, H., & Grönvold, K. (2000). Plagioclase ultraphyric basalts in Iceland: The mush of the rift. *Journal of Volcanology and Geothermal Research*, *98*, 1–32. https://doi.org/10.1016/S0377-0273(99)00189-4

Huber, C., Bachmann, O., & Dufek, J. (2010). The limitations of melting on the reactivation of silicic mushes. *Journal of Volcanology and Geothermal Research*, *195*(2–4), 97–105. https://doi.org/10.1016/j.jvolgeores.2010.06.006

Huppert, H. E., & Sparks, R. S. J. (1989). Chilled margins in igneous rocks. *Earth and Planetary Science Letters*, *92*(3–4), 397–405. https://doi.org/10.1016/0012-821X(89)90063-0

Jakobsson, S. P. (1972). Chemistry and distribution pattern of recent basaltic rocks in Iceland. *Lithos*, *5*(4), 365–386. https://doi.org/10.1016/0024-4937(72)90090-4

Jarvis, P. A., Pistone, M., Secretan, A., Blundy, J. D., Cashman, K. V., Mader, H. M., & Baumgartner, L. P. (2021). Crystal and volatile controls on the mixing and mingling of magmas. In M. Masotta, C. Beier, & M. Silvio (Eds.), *Crustal magmatic system evolution: Anatomy, architecture, and physico-chemical processes* (pp. 125–150). American Geophysical Union. https://doi.org/10.1002/9781119564485.ch6

Jóhannesson, H., & Sæmundsson, K. (2009). *Geological map of Iceland, 1:600000. Tectonics*. Icelandic Institute of Natural History.

Jóhannesson, H., & Sæmundsson, K. (2014). *Geological map of Iceland, 1:600000. Bedrock geology*. Icelandic Museum of Natural History.

Jónasson, K. (2007). Silicic volcanism in Iceland: Composition and distribution within the active volcanic zones. *Journal of Geodynamics*, *43*(1), 101–117. https://doi.org/10.1016/j.jog.2006.09.004

Keiding, J. K., & Sigmarsson, O. (2012). Geothermobarometry of the 2010 Eyjafjallajökull eruption: New constraints on Icelandic magma plumbing systems. *Journal of Geophysical Research: Solid Earth*, *117*(3), B00C09. https://doi.org/10.1029/2011JB008829

Kennedy, B. M., Holohan, E. P., Stix, J., Gravley, D. M., Davidson, J. R. J., & Cole, J. W. (2018). Magma plumbing beneath collapse caldera volcanic systems. *Earth-Science Reviews*, *177*(December 2017), 404–424. https://doi.org/10.1016/j.earscirev.2017.12.002

LeBas, M. J., Maitre, R. W. L., Streckinson, A., & Zanettin, B. (1986). A Chemical classification of volcanic rocks based on the total alkali-silica diagram. *Journal of Petrology*, *27*(3), 745–750. https://doi.org/10.1093/petrology/27.3.745

Magee, C., Hunt-Stewart, E., & Jackson, C. A.-L. (2013). Volcano growth mechanisms and the role of sub-volcanic intrusions: Insights from 2D seismic reflection data. *Earth and Planetary Science Letters*, *373*, 41–53. https://doi.org/10.1016/j.epsl.2013.04.041

Marti, J., & Folch, A. (2005). Anticipating volcanic eruptions. In G. G. J. Ernst (Ed.), *Volcanoes and the environment* (pp. 90–120). Cambridge University Press.

Mattsson, T., Burchardt, S., Almqvist, B. S. G., & Ronchin, E. (2018). Syn-emplacement fracturing in the Sandfell Laccolith, Eastern Iceland—Implications for Rhyolite intrusion growth and volcanic hazards. *Frontiers of Earth Science*, *6*(February). https://doi.org/10.3389/feart.2018.00005

Mattsson, T., Burchardt, S., Mair, K., & Place, J. (2020). Host-rock deformation during the emplacement of the Mourne Mountains granite pluton: Insights from the regional fracture pattern. *Geosphere*, *16*(1), 182–209. https://doi.org/10.1130/GES02148.1

McGarvie, D. W. (1984). Torfajökull: A volcano dominated by magma mixing. *Geology*, *12*(11), 685. https://doi.org/10.1130/0091-7613(1984)12<685:TAVDBM>2.0.CO;2

McGarvie, D. W., Macdonald, R., Pinkerton, H., & Smith, R. L. (1990). Petrogenetic evolution of the Torfajökull volcanic complex, Iceland II. The role of magma mixing. *Journal of Petrology*, *31*(2), 461–481. https://doi.org/10.1093/petrology/31.2.461

Miller, C. F., & Miller, J. S. (2002). Contrasting stratified plutons exposed in tilt blocks, Eldorado Mountains, Colorado River Rift, NV, USA. *Lithos*, *61*(3–4), 209–224. https://doi.org/10.1016/S0024-4937(02)00080-4

Morgavi, D., Arienzo, I., Montagna, C., Perugini, D., & Dingwell, D. B. (2017). Magma mixing: History and dynamics of an eruption trigger. In *Advances in Volcanology* (pp. 123–127). https://doi.org/10.1007/11157_2017_30

Murphy, M. D., Sparks, R. S. J., Barclay, J., Carroll, M. R., Lejeune, A.-M., Brewer, T. S., et al. (1998). The role of magma mixing in triggering the current eruption at the Soufriere Hills Volcano, Montserrat, West Indies. *Geophysical Research Letters*, *25*(18), 3433–3436. https://doi.org/10.1029/98GL00713

National Academies of Sciences Engineering and Medicine. (2017). *Volcanic eruptions and their repose, unrest, precursors, and timing*. National Academies Press. https://doi.org/10.17226/24650

Padilla, A. (2015). *Elemental and isotopic geochemistry of crystal-melt systems: Elucidating the construction and evolution of silicic magmas in the shallow crust, using examples from southeast Iceland and southwest USA. PhD Dissertation*. Vanderbilt University.

Padilla, A. J., Miller, C. F., Carley, T. L., Economos, R. C., Schmitt, A. K., Coble, M. A., et al. (2016). Elucidating the magmatic history of the Austurhorn silicic intrusive complex (southeast Iceland) using zircon elemental and isotopic geochemistry and geochronology. *Contributions to Mineralogy and Petrology*, *171*(8–9), 1–21. https://doi.org/10.1007/s00410-016-1279-z

Passmore, E., Maclennan, J., Fitton, G., & Thordarson, T. (2012). Mush disaggregation in basaltic magma chambers: Evidence from the ad 1783 Laki eruption. *Journal of Petrology*, *53*(12), 2593–2623. https://doi.org/10.1093/petrology/egs061

Paterson, S. R., Pignotta, G. S., & Vernon, R. H. (2004). The significance of microgranitoid enclave shapes and orientations. *Journal of Structural Geology*, *26*(8), 1465–1481. https://doi.org/10.1016/j.jsg.2003.08.013

Petrelli, M., Perugini, D., & Poli, G. (2006). Time-scales of hybridisation of magmatic enclaves in regular and chaotic flow fields: Petrologic and volcanologic implications. *Bulletin of Volcanology*, *68*(3), 285–293. https://doi.org/10.1007/s00445-005-0007-8

Pistone, M., Blundy, J., & Brooker, R. A. (2017). Water transfer during magma mixing events: Insights into crystal mush rejuvenation and melt extraction processes. *American Mineralogist*, *102*(4), 766–776. https://doi.org/10.2138/am-2017-5793

Rhodes, E., Barker, A. K., Burchardt, S., Hieronymus, C., Rousku, S., Mcgarvie, D., et al. (2021). Geochemistry and 3D reconstruction dataset for the Reyðarártindur Pluton, Iceland [Data set]. Zenodo. https://doi.org/10.5281/zenodo.4923170

Rooyakkers, S. M., Stix, J., Berlo, K., Petrelli, M., & Sigmundsson, F. (2021). Eruption risks from covert silicic magma bodies. *Geology*, *49*, 921–925. https://doi.org/10.1130/G48697.1

Sæmundsson, K. (1979). Outline of the geology of Iceland. *Jökull Journal*, *29*, 7–28.

Saubin, E., Kennedy, B., Tuffen, H., Nichols, A. R. L., Villeneuve, M., Bindeman, I., et al. (2021). Textural and geochemical window into the IDDP-1 rhyolitic melt, Krafla, Iceland, and its reaction to drilling. *GSA Bulletin*, *1*, 1–16. https://doi.org/10.1130/b35598.1

Schattel, N., Portnyagin, M., Golowin, R., Hoernle, K., & Bindeman, I. (2014). Contrasting conditions of rift and off-rift silicic magma origin on Iceland. *Geophysical Research Letters*, *41*(16), 5813–5820. https://doi.org/10.1002/2014GL060780

Schipper, C. I., Castro, J. M., Kennedy, B. M., Tuffen, H., Whattam, J., Wadsworth, F. B., et al. (2021). Silicic conduits as supersized tuffisites: Clastogenic influences on shifting eruption styles at Cordón Caulle volcano (Chile). *Bulletin of Volcanology*, *83*(2). https://doi.org/10.1007/s00445-020-01432-1

Schneider, C. A., Rasband, W. S., & Eliceiri, K. W. (2012). NIH Image to ImageJ: 25 years of image analysis. *Nature Methods*, *9*(7), 671–675. https://doi.org/10.1038/nmeth.2089

Scott, J. A. J., Pyle, D. M., Mather, T. A., & Rose, W. I. (2013). Geochemistry and evolution of the Santiaguito volcanic dome complex, Guatemala. *Journal of Volcanology and Geothermal Research*, *252*, 92–107. https://doi.org/10.1016/j.jvolgeores.2012.11.011

Sigmundsson, F., Hreinsdóttir, S., Hooper, A., Árnadóttir, T., Pedersen, R., Roberts, M. J., et al. (2010). Intrusion triggering of the 2010 Eyjafjallajökull explosive eruption. *Nature*, *468*(7322), 426–432. https://doi.org/10.1038/nature09558

Sigurdsson, H., & Sparks, R. S. J. (1981). Petrology of Rhyolitic and mixed magma ejecta from the 1875 eruption of Askja, Iceland. *Journal of Petrology*, *22*(1), 41–84. https://doi.org/10.1093/petrology/22.1.41

Singer, B. S., Jicha, B. R., Harper, M. A., Naranjo, J. A., Lara, L. E., & Moreno-Roa, H. (2008). Eruptive history, geochronology, and magmatic evolution of the Puyehue-Cordon Caulle volcanic complex, Chile. *The Geological Society of America Bulletin*, *120*(5–6), 599–618. https://doi.org/10.1130/B26276.1

Sparks, R. S. J., Annen, C., Blundy, J. D., Cashman, K. V., Rust, A. C., & Jackson, M. D. (2019). Formation and dynamics of magma reservoirs. Philosophical Transactions of the Royal Society A: *Mathematical, Physical and Engineering Sciences*, *377*(2139). https://doi.org/10.1098/rsta.2018.0019

Sparks, S. R. J., Sigurdsson, H., & Wilson, L. (1977). Magma mixing: A mechanism for triggering acid explosive eruptions. *Nature*, *267*(5609), 315–318. https://doi.org/10.1038/267315a0

Storm, S., Shane, P., Schmitt, A. K., & Lindsay, J. M. (2012). Decoupled crystallization and eruption histories of the rhyolite magmatic system at Tarawera volcano revealed by zircon ages and growth rates. *Contributions to Mineralogy and Petrology*, *163*(3), 505–519. https://doi.org/10.1007/s00410-011-0682-8

Streck, M. J. (2008). Mineral textures and zoning as evidence for open system processes. *Reviews in Mineralogy and Geochemistry*, *69*(1983), 595–622. https://doi.org/10.2138/rmg.2008.69.15

Tarasewicz, J., White, R. S., Woods, A. W., Brandsdóttir, B., & Gudmundsson, M. T. (2012). Magma mobilization by downward-propagating decompression of the Eyjafjallajökull volcanic plumbing system. *Geophysical Research Letters*, *39*(19), 1–5. https://doi.org/10.1029/2012GL053518

Thordarson, T., & Hoskuldsson, A. (2008). Postglacial volcanism in Iceland. *Jökull Journal*, *58*(58), 197–228.

Thordarson, T., & Larsen, G. (2007). Volcanism in Iceland in historical time: Volcano types, eruption styles and eruptive history. *Journal of Geodynamics*, *43*(1), 118–152. https://doi.org/10.1016/J.JOG.2006.09.005

Twomey, V., Mcarthy, W., Magee, C., & Petronis, M. (2020). Pre-existing fault-controlled eruptions from the lateral tips of a laccolith in SE Iceland. In *EGU general assembly: Session GMPV9.5 volcanic processes: Tectonics, deformation, unrest*.

Wagner, T., & Lipinski, H. (2013). IJBlob: An ImageJ library for connected component analysis and shape analysis. *Journal of Open Research Software*, *1*(1), e6. https://doi.org/10.5334/jors.ae

Walker, G. P. L. (1960). Zeolite Zones and Dike distribution in relation to the structure of the Basalts of Eastern Iceland. *The Journal of Geology*, *68*(5), 515–528. https://doi.org/10.1086/626685

Walker, G. P. L. (1964). Geological investigations in eastern Iceland. *Bulletin Volcanologique*, *27*(1), 351–363. https://doi.org/10.1007/BF02597532

Walker, G. P. L. (1966). Acid volcanic rocks in Iceland. *Bulletin Volcanologique*, *29*(1), 375–402. https://doi.org/10.1007/BF02597164

Weidendorfer, D., Mattsson, H. B., & Ulmer, P. (2014). Dynamics of magma mixing in partially crystallized magma chambers: Textural and petrological constraints from the basal complex of the Austurhorn intrusion (SE Iceland). *Journal of Petrology*, *55*, 1865–402. https://doi.org/10.1093/petrology/egu044

Wiebe, R. A. (2016). Mafic replenishments into floored silicic magma chambers. *American Mineralogist*, *101*(2), 297–310. https://doi.org/10.2138/am-2016-5429

Zierenberg, R. A., Schiffman, P., Barfod, G. H., Lesher, C. E., Marks, N. E., Lowenstern, J. B., et al. (2013). Composition and origin of rhyolite melt intersected by drilling in the Krafla geothermal field, Iceland. *Contributions to Mineralogy and Petrology*, *165*(2), 327–347. https://doi.org/10.1007/s00410-012-0811-z